Chemical Physics Impact 5 (2022) 100130

Contents lists available at ScienceDirect

Chemical Physics Impact

journal homepage: www.sciencedirect.com/journal/chemical-physics-impact

Investigating the physicochemical properties and pharmacokinetics of curcumin employing density functional theory and gastric protection

Suhailah Wasman Qader [a,*], A. Suvitha [b], Mehmet Ozdemir [c], Innocent Benjamin [e,g,*], Anu Sai Ram NSA [d], Martilda U. Akem [e,f], Ahuekwe Eze Frank [e,h], Emereze C. Eluwa [e]

[a] Department of Medical Laboratory Science, Knowledge University, Erbil, Iraq
[b] Department of Physics, CMR Institute of Technology, Bengaluru-560037, Karnataka, India
[c] Department of Dentistry, Tishk International University, Erbil, Iraq
[d] Department of Medicine, Tirunelveli Medical College, Tamil Nadu, India
[e] Computational and Bio-Simulation Research Group, University of Calabar, Calabar, Nigeria
[f] Department of Pure and Applied Chemistry, Faculty of Physical Sciences, University of Calabar, Calabar, Nigeria
[g] Department of Microbiology, Faculty of Biological Sciences, University of Calabar, Calabar, Nigeria
[h] Department of Biological Sciences, Covenant University

ARTICLE INFO

Keywords:
Curcumin
Pharmacokinetics
DFT
Gastric protection
Physicochemical characteristics

ABSTRACT

The extraction, isolation as well as theoretical investigation of Cumcuma Xanthoriz (cxz) molecule was evaluated to ascertain the physicochemical properties (pc) of the investigated compound. The plant extracts were isolated and characterized using NMR, FT-IR and UV-Vis Spectroscopy study. Pre-geometry characterization as well as theoretical analysis were performed within the frame of density functional theory (DFT) at B3LYP/6-311++ G (d,p) level of theory. Global descriptors were calculated at the same level of theory to ascertain the molecular stability, chemical reactivity of the investigated molecules. Stabilization studies was conducted to properly evaluate the stability of the complex and as such, the result obtained divulged that the charge delocalization from sigma (σ) to anti-sigma (σ*) molecular orbital contributed chiefly to the molecular stability of the studied compound. The calculated UV-Vis spectroscopy study reveal that all absorption spectrum occurred at the visible region (400nm-700nm) which correlate with the experimental λmax obtained. Excitation of CXZ was observed to emanate from π→π*electronic transition. Result from the topology and admet properties explicates that CXZ molecule exhibited good ADMET properties and therefore suggests its suitability as potential plant based drug.

1. Introduction

A wide range of biological and pharmacological effects of curcumin have been documented, including anti-inflammatory, antioxidant, antibacterial, anti-diabetic, anti-cancer, anti-rheumatic, anti-thrombotic, and hepato-, nephro-, and cardiac protective effects. Curcumin has been shown to be exceedingly safe, even at very large dosages, in a number of animal models and human investigations [1,2]. The molecule has equally demonstrated to possess potential ingredients for the treatment and prevention of a wide range of human disorders due to its pharmacological safety and efficacy as reported by [3]. Interestingly, curcumin is thought to be a potential component of functional diets. Over the years, findings have demonstrated curcumin's hyperglycemic action, pointing to the possibility of using curcumin in foods for people with diabetes [4]. It has also been proven to be a natural compound with multiple uses that is pharmacologically safe and has been shown to have cytoprotective effects on healthy human cells [5]. However, in order to get beyond the solubility and bioavailability issues related to curcumin, computational analysis may be utilized as a guide for pre-formulation prospective. The potential targets of curcumin-modified conjugates (CMCs) in breast cancer cells were identified by molecular docking investigations, which initially stipulated that the clinical constraint of employing curcumin as possible anticancer medications, is established that curcumin conjugates have a considerable anticancer property at a sub-micromolar concentration according to a study by Panda and colleagues [6]. On the other hand, Ahmed et al [7] also examined into the biological effects of curcumin, which revealed that the molecular docking predicted binding modes indicated that curcumin binds with

* Corresponding authors.
E-mail addresses: suhailawasman@gmail.com (S.W. Qader), benjamininnocent53@gmail.com (I. Benjamin).

https://doi.org/10.1016/j.chphi.2022.100130
Received 30 August 2022; Received in revised form 9 November 2022; Accepted 20 November 2022
Available online 25 November 2022

the hCA-1 enzyme, thus suggesting efficient pharmalogical effects on target receptors. Additionally, according to Furlan and colleagues [8], the structural characteristics of these potential compounds were explored using DFT studies, in their studies keto and enol isomers of indole curcumin derivatives were compared and energy analysis suggested that enol isomers were more stable than the keto isomers. Also, it was discovered that the result gotten from the molecular docking shows that the keto form of indole curcumin molecules were efficiently binding with GSK.3B, EGFR, and BCR-ABL proteins which implies that they possess significant anti cancer activity. Kumar, and colleagues [9] further explained that in other to examine and study the potentials of curcunin in cancer prevention and treatment, they carried out systematic absorption studies of curcumin and anti cancer drugs on montmorillnite(MMT) nanoparticles in the presence of amphiptilic polymer (PLGA)and in an aqueous environment to understand the contribution of the layered clay structure using cluster(B97-D), DFT and molecular dynamics (MD) simulation in acidic and natural p^H-media. It was found out that(MMT) has affinity towards either polymers or drug molecules.

However, in order to better understand the structure and reactivity of this potent drug, it is imperative to analyze the nature of many of the biological aspects of this prescription, many of which are yet unknown [10–14]. Although, curcumin has not yet received approval as a medicinal agent despite its efficacy and safety, and its poor bioavailability has been cited as a key issue for this as documented by [15,16]. The main causes of curcumin's poor bioavailability include low absorption, quick metabolism, and swift excretion. The research of illness progression, comprehension of drug-organism interactions, and directing of novel drug discovery are all addressed by network pharmacology, a systems biology approach [17]. Significantly, in recent years, a number of studies have reported the use of advanced computational methods, including density functional theory (DFT), to effectively elucidate the structural and chemical properties of compounds in order to develop therapeutics for a variety of diseases. Additionally, molecular docking is used to accurately take into account the compatibility between the drugs and the target receptors. ADME investigations utilizing software such as SWISSADME, pkcSM, etc. are used to assess the rate at which these compounds are absorbed, distributed, metabolized, and excreted.

Herein, the study employs a high-level computational analysis of Curcumin utilizing density functional theory (DFT) approach optimized at B3LYP/6-311++G(d,p) level of theory. Accurate quantum mechanical studies on Curcumin, are here carried out with the aim to analyze the conformational equilibria, to find the most stable equilibrium structure and to define the nature of the molecular orbitals, particularly the highest occupied and lowest unoccupied (frontier molecular orbital) ones that are important to explain binding characteristic. NMR, UV–vis and FTIR both theoretical and experimental data are employed in the comparison with electronic and conformational properties of Curcumin. These probes must also meet certain topological and ADMET property requirements in order to be of interest and well as the molecular docking analysis. This study predicts the standard physicochemical properties (PC) to account for a variety of Absorption, Distribution, Metabolism, Excretion, and Toxicity (ADMET) parameters including molecular lipophilicity, topology, and the Bioactivity Radar to aid drug development using online servers and well-established commercial software.

2. Experimental

2.1. Synthesis

The dried leaves of Curcuma xanthorrhiza (Roxb) were purchased from Ethno Resources Sdn Bhd (846944-K). The plants were extracted using sterilized-distilled water (SDW)and ethanol (E) in a ratio of 1:20. Adult healthy male Sprague Dawley rats (150-200 g) were obtained from animal house, faculty of medicine, University of Malaya, Kuala Lumpur (Ethics No. PM 07/10/2009 MAA (a) (R)). During the laboratory experiment, rats were provided meticulously and care aligned with respect to the standards addressed in the "Guide for the Care and Use of Laboratory Animals" published by the National Academy of Sciences and published by the National Institute of Health. Briefly, the rats were further separated into two groups after being deprived of food for 24 hrs. The animals were then orally administered with the plant extracts for antiulcer assessment separately the details explained in Tables 1 and 2.

2.2. Spectroscopy

On a Bruker Avance AMX400 spectrometer using a Broad Band 5-mm probe, NMR spectra are captured at 300 K. (inverse detection). The conventional frequencies for 13C and 1H are respectively 100.13 MHz and 400.13 MHz. The following are the typical acquisition parameters for 1 H: Spectral bandwidth (SW) of 20 ppm, pulse width of 6.1 ls (90-pulse hard pulse on 1 H), pulse latency of 0.5–1 s, and scan count of 216–512. Typical settings were employed for 2D H, H-Homonuclear Correlated Spectroscopy (COSY). Appropriate settings were employed for 2D H, X-Hetero Correlated Spectroscopy (HMBC and HMQC). (50–90 pulses; 32 k data points; 1 s relaxation delay; 8–64 k transients; 1 JH–C 125–145 Hz; 3 JH–C 5–15 Hz). The B3LYP approach was used to determine the electronic transition for the CXZ, with the base 6-311++G (d, p) set to UV-visible spectral computation and the gaseous phase included. Between 300 and 800 nm, the theoretical UV-visible absorption spectrum was measured in the gaseous phase.

2.2.1. Computational details

Time-dependent DFT (TD-DFT) calculations were performed on the compound *Curcuma xanthorrhiza* to optimize the structure in the ground state (shown in Fig. 1) at Becke's three-parameter functional and Lee-Yang-Parr hybrid functional (B3LYP) level at 6-311++ G(d, p) basis set using both Gaussian (G09) [18] and GaussView 6 [19] programs. To perform UV-Vis spectral computations that are applied to optimal structures, TD-DFT/B3LYP/6-311++G (d, p) was utilized. Comparative physical indices such as E_{HOMO}, E_{LUMO}, offset HOMO/LUMO, MEP, spin, ionizing-potential (I), electronic-affinity (A), chemical-potential (μ), hardness (η), electrophilic-index (ω), softness (ζ) measurements of the gaseous phase are measured.

2.2.2. Molecular docking details

Herein, the downloaded protein (PDB ID: 1BZM) was prepared using the Biovia Discovery Studio and docked with the compound under investigation (curcumin) and further validated by docking same with the conventional drug (omeprazole). To sequentially prepare the protein before carrying the molecular docking proper, water molecules present in the proteins were deleted and the active binding sites were defined from the current ligand site after which the native ligand present in the protein was deleted. The binding site was expanded to cover more area and the polar hydrogens were added to the structure and saved in PDB format. The sphere's radius and coordinates were copied in order to dock. The PDB formatted proteins that had been saved were chosen from the read molecule tab of the Autodock Vina software. The grid and macromolecule icon were chosen, the protein was chosen as a

Table 1
Effect of aqueous extract of selected Malaysian medicinal plants on ulcer area and percentage inhibition of ethanol induced gastric ulcer rats.

Pre-treated dose (5 mL/kg)	^H_P	Ulcer area(mm)^2 (Mean ± S.E.M)	Inhibition (%)
DW (negative ulcer control)	3.45 ± 0.13	865.3 ± 42.4	-
OMP (positive control 20 mg/kg)	6.84 ± 0.17*	114.4 ± 3.71*	86.77
▓CXLAE (250 mg/kg)	4.03 ± 0.14*	314.9 ± 7.40*	63.60
▓CXLAE (500 mg/kg)	4.50 ± 0.12*	224.9 ± 9.24*	74.00

Table 2
Effect of ethanol extract of selected Malaysian medicinal plants extract on ulcer area and percentage inhibition of ethanol induced gastric ulcer rats.

Pre-treated dose (5 mL/kg)	$^{H}_{P}$	Ulcer area(mm)^2 (Mean ± S.E.M)	Inhibition (%)
CMC (negative ulcer control)	3.60 ± 0.10	978.3 ± 32.4	-
OMP (positive control 20 mg/kg)	6.84 ± 0.17*	114.4 ± 3.71*	88.30
CXLEE (250 mg/kg)	4.25 ± 0.10*	91.10 ± 9.29*	90.68
CXLEE (500 mg/kg)	5.10 ± 0.23*	81.70 ± 7.29*	91.64

macromolecule, and the file was saved in pdbqt format. The required ligand in pdb format was selected once the ligand icon was clicked. The ligand was loaded, and the ligand and output tab was chosen to save the ligand in pdbqt format. Results were acquired using the Biovia discovery studio visualizer.

3. Results and discussions

3.1. Geometry optimization

The highly symmetrical and conjugative nature of Curucuma xanthorhiz (CXZ) accounts for its versatility and utilization in diverse applications. Several derivatives have been isolated and reported. The structure is composed of 8 rotatable bonds interwoven between two aromatic rings with 6 acceptors and 2 donor groups which are responsible for the ease of inter-conversion from the keto to the enol tautomer and vice versa. It is synonymous to the compound 1 1, 6-Heptadiene-3, 5-dione, 1,7-bis(4-hydroxy-3-methoxyphenyl). However, to accurately predict molecular properties and assess the bio-activity of the studied compound, geometry optimization was ensured at the B3LYP functional with the 6-311++G (d, p). The molecule is observed to possess 4 distinct bonds. The C=O bond length is computed to be – while the aromatic C=C bond is observed to be—similarly as well as the OH. The bond lengths suggest therefore that the title compound poses a great inhibitory potential on target receptors.

3.2. NMR spectra

The experimental ^{1}H NMR spectra of the titled compound in DMSO-d_6 as a solvent confirmed the presence of suspect protons. A comparison of the experimental and calculated spectra is represented in **Fig S1** and **S2** of the supporting information. The aromatic protons found in the test compound, for the experimental, appeared at 6.86-7.63 ppm, while the number of protons calculated showed 7.20-8.89 ppm. This depicts the presence of protons among aromatic and heteroaromatic rings duplicated in their expected regions [20,21]. The variations in protons signal may be attributed to varied behaviour to the ions in the compound [22]. The ^{1}H NMR integration curves confirms the formation of keto-enol tautomers of the proposed structures in solution.

3.3. UV–visible& DOS spectral analysis

The results of the Gauss Sum software analysis of key contributions to electronic transfers are summarized in Table 3. Excitation energies E (eV) and oscillator strengths (f) were measured, as well as experimental absorption wavelength (nm) and major contribution (HOMO-LUMO). Fig. **S3** of the supporting information depicts a pictorial representation of theoretical UV-Vis Spectra and a DOS chart. While the investigated CXZ exhibited six absorption bands in the theoretical UV spectrum at 417,371,370,358,349 and 322 nm, this corresponded duly with the experimental λ (nm) as shown in Table 3. These results suggest that the investigated compound may be attributed to the aromatic, amino benzoate anion, monohydrate and oxalate moiety, respectively, these transformations could be contributed to the π→π*, n→π*, σ→σ* transition.

Table 3
Absorption wavelength λ (nm), excitation energies E (ev) and oscillator strengths (f) theoretical and experimental electronic absorption spectra using the process TD-DFT / B3LYP/6-311++ (d, p).

Molecule	λ (nm) Experimental	Theoretical λ(nm) Computed	E (eV)	*f* (a.u)	Major contribution
CXZ	416.8	417.3	2.96	0.0205	HOMO->LUMO (91%)
	421.3	471.2	3.33	0.3351	H-1->LUMO (85%)
	419.5	422.1	3.34	0.0175	H-5->LUMO (26%), H-3->LUMO (23%), H-2->LUMO (31%)
	358.0	375.1	3.45	0.0006	H-3->L+1 (68%), H-2->L+1 (21%)
	358.4	349.4	3.54	0.2495	HOMO->L+1 (88%)
	343.8	322.1	3.84	0.0003	H-1->L+1 (97%)

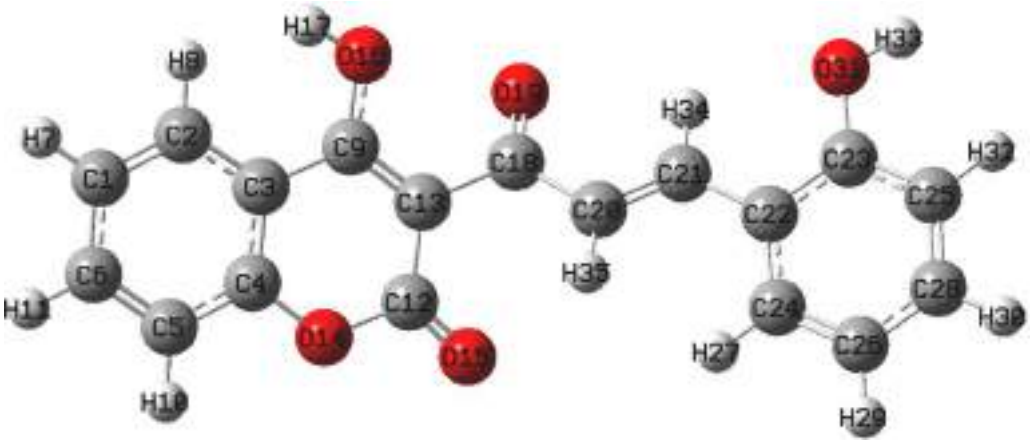

Fig. 1. Optimized Molecular Structure of CXZ.

3.4. Vibrational Analysis

Vibrational analyses aid in qualitative and quantitative characterization of test compounds. The FT-IR analysis assessed the functional group types present in the test compound, via distinct molecular vibrational bands for the respective functional groups present. The computationally calculated vibrational wavenumbers and experimental (FT-IR) measurements of the titled compound are presented in Table 4 and the spectra is illustrated in fig. S4 of the supporting information. To improve agreement between the theoretical and experimental values, and to compensate for the errors possibly arising from the basis set, the computed harmonic frequencies in line with their potential energy distribution are generally scaled for comparison [23]. However, observed slight variations could be attributable to solvation and different functional effects [24].

C – H vibrations:

Vibrational bands in aromatic compounds reveal C-H stretch peaks normally in the region of 2850-3100 cm^{-1} [25]. More so, the nature and position of substituents affect these vibrations. In this study, the experimental C-H stretch deformations were observed at 808.03, 960.38, 1025.87 and 1112.73 cm^{-1}, with the corresponding theoretical C-H stretch values giving 969.07, 1017.08, 1030.4 and 1119.81 cm^{-1}, respectively. This data shows the closeness of the calculated theoretical values to the experimental results. Significant wavelength deviations from the norm could arise from solvent effects, as well as antisymmetric stretching vibrations of aldehyde bonds due to varying bond lengths. Thus, leading to weak absorption peaks [26]. Another possible explanation would be that the vibrational shift of the CH bond interacting with metals (or other elements) was averaged out by the unchanged vibrational mode of the non-interacting CH bonds; indicated by weakened bonds which inadvertently result in a reduced wavelength [27].

C – C vibrations

C – C vibrations arise in the range between 1300-1000 cm^{-1} [28]. In this study, the experimental σC=C stretching vibration frequency deformations occurred at 1135.89 and 1151.30 cm^{-1} and theoretically at 1178.58 and 1183.46 cm^{-1}, respectively. For τ C = C, experimental and theoretical values fell at 1182.18 and 1201 cm^{-1}, respectively; while ωC = C reported 1203.39, 1232.72, 1274.73, and 1263.98, 1281.71, 1301.60 cm^{-1} for experimental and theoretical values respectively. Theoretical values were in good agreement with the experimental results.

C-O vibrations

The stretching frequency varied in both the symmetric and asymmetric bond types. Experimental and Theoretical vibration frequencies with $_{Sym}$C = O were observed at 1427.08, 1600.67, 1625.74, and 1435.06, 1801.30, 1837.93 cm^{-1}, respectively; while the υ_{AS}C = O gave 1506.17, 1587.16, and 1549.97, 1637.77 cm^{-1}, for both the experimental and theoretical values, respectively. Previous studies have reported variable C-C band stretches [29]. However, close theoretical values and experimental data were reported in this study.

O-H vibrations

The presence of inter or intra molecular hydrogen bonding in the molecules of O-H group makes for a large variation in wavenumber, intensity and bandwidth of the spectral vibrations. As such the O-H stretching vibration is expected in the wide range of 3380 ± 200 cm^{-1} [24,25]. For the theoretical values of the title compound appearing at 3903.04 and 3906.59, the υO – H stretching for the experimental data were in good agreement as pure stretching mode at 2846.48 and 3507.92 cm^{-1}.

Table 4
Analysis of the theoretical and experimental vibrational frequencies of curcumin.

Experimental	Absorbance	Theoretical	Transmittance	Assignment with PED%
808.03	0.482	969.07	1.45	υ_{AS}C-H (-75)
960.38	0.485	1017.08	0.26	υ_{AS}C-H (-79)
1025.87	0.442	1030.40	42.47	υ_{AS}C-H (-81)
1112.73	0.497	1119.81	45.74	υ_{AS}C-H (-79)
1135.89	0.451	1178.58	16.62	δC=C (38)
1151.30	0.614	1183.46	7.35	δ C = C (31)
1182.18	0.457	1201.50	31.02	τ C = C (48)
1203.39	0.488	1263.98	202.03	ωC = C (37)
1232.72	0.383	1281.71	22.55	ωC = C (28)
1274.73	0.384	1301.60	76.33	ωC = C (49)
1427.08	0.477	1435.06	210.61	υO=C (24)
1506.17	0.491	1549.97	74.69	υO=C (30)
1587.16	0.212	1637.77	180.85	υO=C (29)
1600.67	0.249	1801.30	215.72	υO=C (34)
1625.74	0.242	1837.93	713.65	υO=C (36)
2846.48	0.049	3903.04	105.58	υO – H (49)
3507.92	0.085	3906.59	110.96	υO – H (55)

3.3. Frontier Molecular orbital (FMO) analysis

The HOMO and LUMO energy values can be used to determine a molecule's ability to donate and receive electrons. Electrical and optical properties, luminescence, photochemical reactions, UV-VIS, quantum chemistry, and pharmaceutical research, as well as providing information on biological mechanisms, rely on these molecular orbitals [26–28]. Frontier molecular orbitals (FMOs) energies such as I=-Energy HOMO and A= -Energy LUMO, according to Koopmans' definition, measure ionization1 potential (I) and electron affinity (A). A compound's chemical reactivity is believed to be determined by the energy gap, which is established by the difference between the energies of HOMO-LUMO. It has been demonstrated that a molecule's energy gap impacts its chemical reactivity, biological activity, polarizability, and susceptibility to bind compounds to target receptors [29]. The investigated compound revealed a very significant energy gap of 3.437 eV which in comparison with other literatures suggest that this compound possesses sufficient biological properties [30]. This assertion was significantly supported by the slight decrease in energy gap (2.886 eV) established in the docked complex with a difference of 0.551 eV. Importantly, a study carried out by Das and colleagues [31] revealed that at the binding site, the HOMO orbitals of the ligand interact with the LUMO orbitals of the amino acid residues. When a complex is formed, however, HOMO orbitals of the binding site residues interact with LUMO orbitals of the ligand. Additionally, the active site loop of Lys213, Glu214, Lys149, and Ser217 were found to be essential for binding of the drug candidate due to its significant atomic displacements and intra-molecular hydrogen bonding. Herein, with the aid of the energies of the HOMO and LUMO orbitals, other examinations of the investigated molecule's chemical reactivity parameters, including chemical softness (S), chemical potential (μ), electrophilicity index (ω), and chemical hardness (η), were also performed as shown in Table 5. Additionally,

Table 5
Analysis of the electronic properties of CXZ.

Parameters	B3LYP_6–311++G(d,p)
Electronic spatial extent (au)	21174.8
nuclear repulsion energy (Hartree)	2110.17
Rotational coefficients (GHz)	0.2857
	0.053
	0.047
Dipole moment	2.611debye
Parameters	
$\mathbf{E_{LUMO}}$ (eV)	-2.6716
$\mathbf{E_{HOMO}}$ (eV)	-6.1086
Energy Gap (eV)	3.437
$\mathbf{I = -E_{HOMO}}$ (eV)	6.1086
$\mathbf{A = -E_{LUMO}}$ (eV)	2.6716
$\eta = \frac{1}{2}(E_{LUMO}-E_{HOMO})$ (eV)	1.7185
$\mu = \frac{1}{2}(E_{LUMO}+E_{HOMO})$ (eV)	-4.3901
$\psi = \mu^2/2\eta(eV)$	5.607
$\zeta = 1/\eta(eV^{-1})$	0.5819

according to [32], a molecule's electrophilicity index provides information regarding how well a substance can bind to biomolecules. The molecule in question has a higher electrophilicity index value, indicating that it can act as an electrophilic species and has a greater ability to bind to biomolecules and thus, confirms the pathway for molecular docking approach with different protein targets. Conversely, a soft molecule with strong polarizability has a lower chemical hardness value and a higher negative electrochemical potential (μ) indicates a chemical species' willingness to accept electrons while electronegativity (χ) measures the capacity of an atom/group of atoms to attract electrons in the molecule. Interestingly, results calculated validated the biological relevance of the compound under investigation as shown in Table 4. More so, the electron occupied and unoccupied (electron affinity and donating) sites are shown in 3D representations of FMO orbitals in different transitions (HOMO-LUMO) levels in Fig. 2.

3.4. Natural Bond Orbital (NBO) analysis

The NBO analysis relies on a series of methods that allow for the extraction of fundamental bonding concepts from density functional theory (DFT) calculations. It facilitates the conversion of the Schrodinger's wave equations' computational keys [33,34]. For the clarification of hyperconjugative interactions and the delocalization of electron density in the solvent, natural bond orbital analysis is a suitable tool. It is also a reliable technique for analyzing intra- and intermolecular bonding and interactions within bonds. The second- order perturbation theory analysis of the Fock matrix was carried out to evaluate the donor-acceptor interactions in the NBO basis. The concentration of the donor-acceptor interaction was denoted by the second order stabilization energy, E^2. The larger value of E^2 indicates the stronger interaction between electron donors (i) and the electron acceptor (j) which signifies a more donating propensity from an electron donor to electron acceptor and hence, a higher degree of conjugation of the whole system [35]. NBO can be mathematically expressed as outlined in literature [36]

NBO analysis of the studied molecule, is tabulated in Table 6 showing a strong intermolecular hyper conjugative interaction. From the computational details, it is observed that the studied compound had highest donor to acceptor interaction from (donor) σC_{20} - C_{21} → σ*C28 - H30 (acceptor), σC_{18} - C_{20} → σ*C26 - C28, σC_{20} - H35→ *σC26 - C28

Table 6
Analysis of the natural bond orbital at.

Donor orbital	Occupancy	Acceptor orbital	Occupancy	E^2 Kcal/mol	E(j)-E(i)	F(i,j)
σC_{20} - C_{21}	1.98490	σ*C28 - H30	0.01051	594.04	1.89	0.946
σC_{18} - C_{20}	1.98338	σ*C26 - C28	0.02072	577.05	1.85	0.923
σC_{20} - H35	1.93623	*σC26 - C28	0.02072	427.47	1.58	0.741
σC_{20} - C21	1.98490	*σC26 - C28	0.02072	434.82	1.84	0.799
σC_{20} - H35	1.93623	*σC28 - H30	0.01051	405.90	1.63	0.736
σC18 - C20	1.98338	*σC28 - H30	0.01051	403.37	1.90	0.783
LP(1)O 15	1.97733	*σC26 - C28	0.02072	183.90	1.94	0.533
π*C2 - C3	0.27819	*πC1 - C6	0.20847	107.82	0.02	0.076
πC_{20} - C21	1.85399	*σC28 - H30	0.01051	98.11	1.43	0.346
LP(2)O 15	1.86743	*σC26 - C28	0.02072	91.37	1.44	0.333

which is found to have the highest the stabilization interaction of 594.04 Kcal/mol, while the occupancies explain the location of the donor electron or orbital in an atom. Hence, the interaction is between sigma bond to the sigma anti-bonding contributing greatly to the stability of the compound (cmr). Relatively, the highest perturbation energy results from the influence of the antibonding interaction between atoms, amounting in the increased molecular stability as seen in other stability descriptors. These stabilization interactions between the lone pair orbitals and the antibonding orbitals increases the stability of these compounds.

3.5. Mulliken and Natural Population Analysis (npa)

The natural population analysis accurately determined the distribution of electrons in various subshells of their atomic orbitals and their occupancies [37]. The system of natural population analysis has been established to estimate the atomic charges and orbital populations of

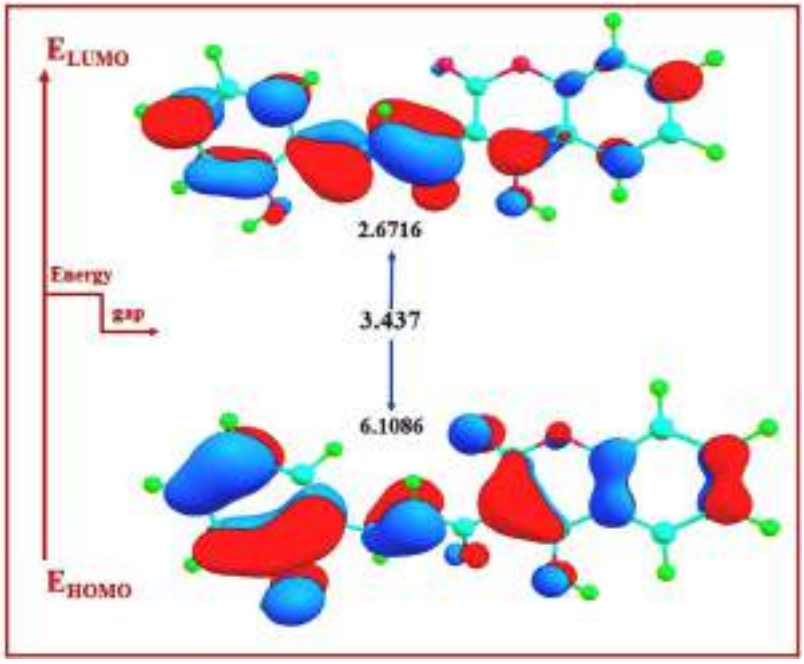

Fig. 2. DFT/B3LYP/6–311++G(d,p)-3D representations of FMO orbitals in (HOMO-LUMO) levels for CXZ.

molecular wave functions. Natural analysis is also an alternative to predictable Mulliken population analysis which appears to unveil and enhanced the numerical stability and to better describe the electron distribution in compounds of high ionic character, such as those comprising metal atoms [38]. These charges are seen to affect the properties like dipole moment, electronic parameters, polarizability, and refractivity [39]. The iso-surface of molecular electrostatic potential, determines the interacting strength of the compound, it is considered suitable for the prediction of the reactivity of the molecule towards nucleophilic and electrophilic occurrences [40–43]. It also predicts which category of intermolecular interactions is possible within the interacting system. From our studies, red color best explains the presence of dispersion force and negative charges with higher electron density, blue represent a positive charge with less electrostatic potential (electrophilic) while yellow signifies negative charge where high electrostatic potential resides.

On the other hand, the Mulliken population analysis, describes the distribution of the charges in the various sub shells in the molecular orbital. The atomic charge influences the polarizability, dipole moment, electronic structure and many other molecular properties of the system [36]. As reported in table S1 of the supporting information and Fig. 3. The Mulliken atomic charge can also be employed for the characterization of the electronic charge distribution in a particular molecule and also for the characterization of the bonding, antibonding and non-bonding nature of the molecular orbitals [37]. Herein, the Mulliken atomic charges cover a broad range of values from -0.429144 at the low side to 1.002035 at the high side at the Hartree-Fock level. The atoms C_3, H_7, H_8, C_9, H_{10}, H_{11}, C_{12}, C_{13}, H_{17}, C_{18}, C_{21}, C_{22}, C_{23}, H_{27}, H_{29}, H_{30}, H_{32}, H_{33}, H_{34}, and H_{35} respectively have positive charges and the atoms C_1, C_2, C_4, C_5, C_6, O_{14}, O_{15}, O_{16}, O_{19}, C_{20}, O_{24}, O_{25}, O_{26}, O_{28}, O_{31}, have negative charges. The hydroxyl oxygen O_{15} is more negative with value -0.429144 eV which is proved very strongly in Fig. 3.

3.6. Molecular electrostatic potential analysis

The MESP surface is extremely useful for understanding the potential sites for electrophilic (negative region) and nucleophilic (positive region) reactions [44,44], and it is particularly well suited for recognising one molecule by another via this potential and density, as shown in Fig. 4. Different shades represent the electrostatic potential levels at the surface in the order red > orange > yellow > gree n> blue. In the named compound, the colour code for these maps ranges from -1.533e^{-2} (deepest red) to +1.533e^{-2} (deepest blue), with blue representing the most electropositive, i.e. electron poor region, and red representing the most electronegative, i.e. electron rich region. The most electronegative region in the molecule is clearly around the three oxygen atoms, which act as an electron donor.

3.7. In silico ADMET analysis

According to the Lipinski's rule, which was used to clearly and unequivocally explain the drug-likeness and bioavailability capabilities of the investigated compound, it was examined that the compounds' absorption, distribution, metabolism, excretion, and toxicity properties made it clear that the molecules possess very reasonable pharmacokinetic features. This standard helps to assess the likelihood that a biologically active compound will have the chemical and physical properties required for absorption and bioavailability. The Lipinski rule is based on pharmacokinetic drug properties including molecular mass less than 500 Da, partition coefficient not greater than 5, and a maximum of 5 donors and 10 acceptors for hydrogen bonds. CXZ had a 368.38g/mol molecular weight. As a result, the Lipinski rule of five was strengthened by the findings that the minimum reported number of hydrogen bond donors was successful for oral administration. This outcome was in line with the information found on the number of hydrogen bond acceptors, which is provided in table X of the supporting data. In light of this, it is crucial to point out that after carefully examining the investigated compound, it is relevant to say that the molecule didn't violate any requirements, which implies that the molecule has excellent potential as an antimicrobial.

Additionally, no abnormalities in gastrointestinal (GI) absorption, blood brain barrier (BBB) permeability (a term used to describe the unique characteristics of the central nervous system (CNS) of microvasculature), P-gp substrate, CYPIA2, CYP2CI9, CYPP2D6, CYP3A4, Ghose, Veber, Egan, or Muegg were found by this examination, indicating that the molecule represents high hydrophilic properties and polar chemical as shown in Table 7. Therefore, the high potency, affinity, and selectivity against the molecular target were assessed in order to better understand the risky characteristics of the tested drugs. This led to the conclusion that CXZ was unlikely to be carcinogenic, mutagenic,

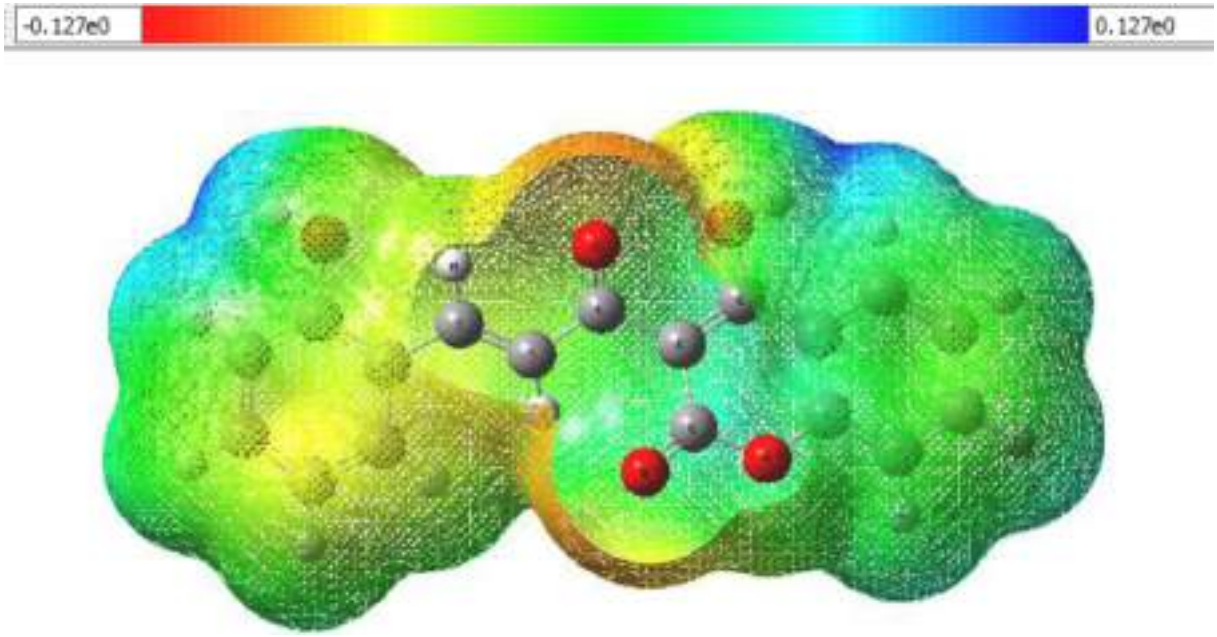

Fig. 3. Plot illustrating the mulliken and natural population analysis.

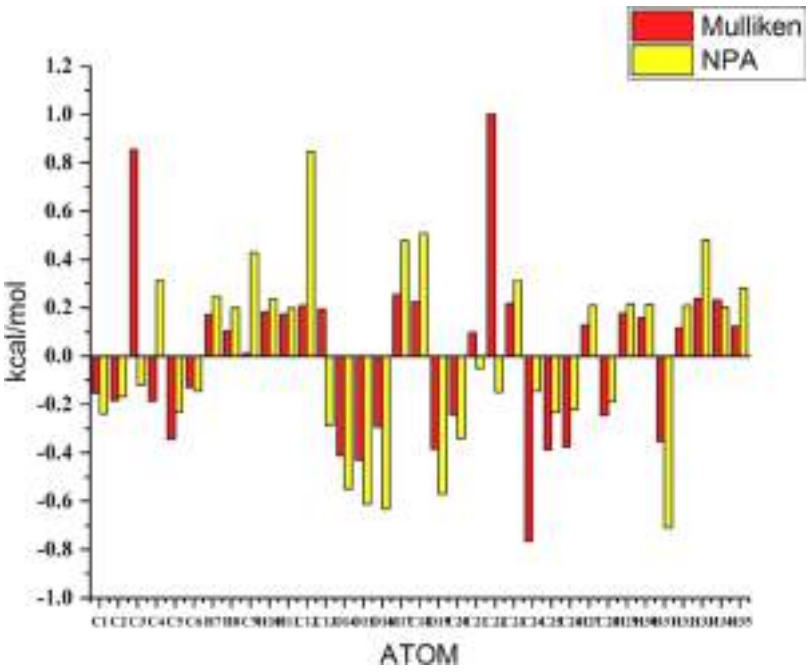

Fig. 4. Molecular electrostatic potential of studied CXZ compound.

or cytotoxic, with likelihood values of 0.62, 0.97, and 0.93, respectively as shown in table S8 of the supporting information. Significantly, this discovery implies that the lead compound possesses antimicrobial properties. The methoxy phenyl and heptadiene dione rings, which are highly significant in the antimicrobial activity, may be the source of this compound's remarkable biological power. The bioavailability radar, on the other hand, is shown to quickly assess how drug-like the molecule is.

3.8. Gastric Ulcer Assessment; Ethanol Induction Model

All the aqueous and ethanol plant extract were evaluated for gastroprotective capability. The results showed that all the aqueous and ethanol plant extract were significantly ($P<0.05$) inhibited ulcer area against ethanol induction model in comparison to negative control group. Rats pretreated with 500 mg/kg of *C. xanthorrhiza* leaf ethanol extract CXLEE were protected stomach with 91.64 % while rats pretreated with *C. xanthorrhiza* leaf aqueous extract CXLAE were inhibited ulcer area with 74.00 %. Macroscobical examination of the gastric mucosa in a rat pre-treated with 5 mL/kg of 20 mg/kg OMP and 250 mg/kg and 500 mg/kg CXLEE showed moderate injuries in the gastric mucosa in comparison with CMC negative control group. It was also observed that histological examination of the stomach of rats pretreated with CMC suffered markedly extensive damage to the gastric mucosal layer with edema and leukocyte infiltration of the submucosal layer. Rats pre-treated with 5 ml/kg of 20 mg/kg omeprazole showed mild disruption to surface epithelium mucosa with mild edema and leukocyte infiltration of the submucosal layer. Meanwhile, rats pretreated with 500 mg/kg of CXLEE showed less destruction to the mucosal surface and mild edema and leukocyte infiltration in submucosal layer as shown in Fig. 5.

The p^H of gastric juice was recorded for all groups, the results showed that rats pretreated with negative control group (CMC and DW) have significantly ($P<0.05$) lower p^H (3.45 ± 0.13 and 3.60 ± 0.10 respectively) compared to other groups. While the p^H of gastric juice in the rats pretreated with positive control group OMP and all the plant extract in both aqueous extract (Fig. 4.3) and ethanolic extract were significantly ($P<0.05$) higher pH than negative control group. Rats pretreated with 20 mg/kg of OMP (6.84 ± 0.17) and 500 mg/kg of APLEE (7.18 ± 0.09) and PMLEE (7.22 ± 0.14) as in Table 8 showed elevation of p^H compared to other selected plants.

3.9. Comparative Studies

The antiulcer effect of curcuma xanthorhiza (roxb) was compared with traditional folk medicines used for the effectiveness against ulcer namely Maytenus robusta (Celastraceae), Pithecellobium Jiringa, Achryocline saturoides. The ethanol extract of each of the above plants were compared depending upon the data available under the headings shown in Table 8.

3.10. Medicinal review analysis

Table 9 established the antiulcer effect of curcuma xanthorhiza (roxb) was compared with traditional folk medicines used for the effectiveness against ulcer namely Maytenus robusta (Celastraceae), Pithecellobium Jiringa, Achryocline saturoides. The ethanol extract of each of the above plants were compared depending upon the data available under the following headings p^H, ulcer area, inhibiton %. Curcuma xanthorizha have resulted in the formation of high p^H i.e. 4.25 ±0.10* and 5.10±0.23* respectively at 250mg and 500 mg, indicating the inhibitory effect on gastric mucosa and movement of the p^H scale towards alkaline, indicating a better result when compared with Maytenus robusta which have less p^H i.e. 2.96±0.07* and 2.92±0.15* respectively at 250 mg and 500 mg. Also, while comparing the ulcer area inhibition % Curucuma xanthorhiza have proved to be more efficacious with percentage of 90.68 and 91.64 at 250mg and 500mg respectively, when compared with Prithecellobium Jiringa which have inhibition % of 72.17 and 80.55 at 250 mg and 500 mg respectively. Comparing similarly the data's of Achyrocline satureiodes which have an inhibition % of 58.8±11.5 and 86.2±12.2 at 250mg and 500 mg, which are largely at a low range when compared to that of Curucuma xanthorhiza.

3.11. Molecular docking analysis

On a global scale, molecular docking has been identified as a critical tool for drug design because it aims to explain several modules underlying protein-ligand interaction, which support the process by which proteins interact with small molecules (known as ligands) to form stable

Table 7
Biological activity and physicochemical parameters of CXZ.

Physicochemical Properties		Lipophilicity	
Form.	$C_{21}H_{20}O_6$	Log Po/w (iLOGP)	3.27
Mol. weight	368.38 g/mol	Log Po/w (XLOGP3)	3.20
Num. heavy atoms	27	Log Po/w (WLOGP)	3.15
Fract. Csp3	12	Log Po/w (MLOGP)	1.47
Num. rot. bonds	0.14	Log Po/w (SILICOS-IT)	4.04
Num. H-bond accpt.	8	Consensus Log Po/w	3.03
Num. H-bond donors	6	Log Po/w (iLOGP)	3.27
TPSA	93.06 Å^2	Class	Soluable
PK		**Medicinal Chemistry**	
GI abs.	High	PAINS	0 alert
BBB permeant	No	Brenk	2 alerts: beta_keto_anhydride, michael_acceptor_1
P-gp substrate	No	Lead like ness	No; 2 violations: MW>350, Rotors>7
CYP1A2 inhib.	No	Synthetic accessibility	2.97
CYP2C19 inhib.	No	**Water Solubility**	
CYP2C9 inhib.	Yes	Log_S_(ESOL)	-3.94
CYP2D6 inhib.	No	Solub.	4.22e-02 mg/ml; 1.15e-04 mol/l
CYP3A4 inhib.	Yes	Class	Soluble
Dr.likeness	Yes	Log_S_(Ali)	-4.83
Lipinski	No; 1 violation	Solub.	5.50e-03 mg/ml; 1.49e-05 mol/l
Ghose	Yes	Log_S_ (SILICOS-IT)	-4.45
Veber	No; 1 violation	Solub.	1.31e-02 mg/ml; 3.56e-05 mol/l
Egan	Yes		
Muegge	0.56		
Bio.av. Score	Yes		
Log Kp (skin permeation)	-6.28 cm/s		

Formula, Mol.weight: Molecular weight, Num: Number, Solub.: Solubility, Abs.: Absorption, Inhib.: Inhibitors, Bio.av.score: Bioavailability score, Dr.likeness: Druglikeness, PK: Pharmacokinetics, accpt: acceptor, rot.: rotatable, Fract.: Fraction.

complexes with biologically significant functions [45–50]. Contrarily, protein-ligand complexes are essential for a number of biological functions. In this case, the inhibition of the carbonic anhydrase enzyme is discussed, which is thought to be the main driver of the therapeutic benefits in evaluating ulcer illnesses. According to research by Chakravarty and colleagues [51], carbonic anhydrase interacted with three different sulfonamide drug structures to form complexes that were all bound in the enzyme's active site, but these complexes varied in the ways that their sulfamido groups interacted with the crucial zinc ion. As a result, the current research that led to the selection of this target receptor was made easier and further supported the existence of an active site in the enzyme. At the cellular level, the hydrogen bond plays a critical role in enhancing molecular interaction and compound structural integrity [52]. It also aids in compound solubility and gastrointestinal absorption into the body. Notably, as illustrated in Fig. 6, the active site loop of Lys213, Glu214, Lys149, and Ser217 was determined to be crucial for binding of the lead compound due to its substantial atomic displacements and intra-molecular hydrogen bonding as shown in Fig. 7. The orientation discrepancies of curcumin as well as variations in the inhibitory potencies of the compound was proposed to be caused by these interactions coupled with active site charge requirements. The native enzyme's Lys213, Glu214, Lys149, and Ser21767 active site residues, among others, were observed to form a hydrogen bond network with solvent molecules that was observed to be broken following binding to curcumin. In addition, Lys149 and Ser215 amino acid residues were seen in the interaction between the conventional drug (omeprazole) and the target receptor, which is determined to be comparable to that of curcumin and the target protein. These, however, imply that both amino acid residues are crucial for enhancing the lead compound's inhibitory potentials. However, it was determined that the omeprazole@1BZM interaction contained noteworthy pi-hydrogen bonds, pi sulphur, pi-alkyl, pi-pi T-shaped, and alkyl links. As both CXZ and omeprazole computed relatively identical binding affinities of -5.67 kcal/mol and -5.12 kcal/mol, respectively, this investigation relatively establish that curcumin could as well act as a proton pump inhibitor thus blocking precisely the carbonic anhydrase enzyme used in this investigation.

4. Conclusion

The spectroscopic and pharmaceutical investigations of the ligand were investigated theoretically and experimentally using DFT and the B3LYP/6-311++G(d,p) level of theory. Using NMR, FT-IR, and UV-Vis Spectroscopy studies, the plant extracts were extracted and characterized. Density functional theory (DFT) at the B3LYP/6-311++ G (d,p)

Table 8
p^H, ulcer area, inhibiton %.

		Maytenus robusta	*Curcuma xanthorhiza*	*Pithecellobium Jiringa*	*Achyrocline satureoides*
p^H	250mg	2.96 ± 0.07*	4.25 ± 0.10*	-	-
	500mg	2.92 ± 0.15*	5.10 ± 0.23*	-	-
Ulcer area (mm)2 (Mean ± S.E. M)	control	-			361.2 ± 51.3
	250mg	-	91.10 ± 9.29*	228.17 ± 1.51	25.9 ± 8.5
	500mg	-	81.70 ± 7.29*	156.33 ± 1.84	9.3 ± 8.3
Inhibition % (250mg)		-	90.68	72.17	58.8 ± 11.5
Inhibition % (500mg)		-	91.64	80.55	86.2 ± 12.2

Fig. 5. Macroscopic observation of gastric wall in: (A) rats pre-treated with 5 mL/kg of CMC (negative control), (B) omeprazole (20 mg/kg) positive control group, (C) 5 mL/kg of 250 mg/kg CXLEE and (D) 500 mg/kg of CXLEE. Severe injuries were seen in the gastric mucosa in rats pre-treated with CMC. Injuries to the gastric mucosa were milder in rats pre-treated with omeprazole in comparison to the injuries seen in the CMC pre-treated rat. Moderate injuries are seen in the gastric mucosa (magnification: 1.8X). The white arrow indicates gastric lesion as shown in Fig. 6.

Table 9
Analysis of the medicinal review.

		Maytenus robusta	Curcuma xanthorhiza	Pithecellobium Jiringa	Achyrocline satureoides
p^H	250mg	2.96 ± 0.07*	4.25 ± 0.10*	-	-
	500mg	2.92 ± 0.15*	5.10 ± 0.23*	-	-
Ulcer area $(mm)^2$	control	-			361.2 ± 51.3
(Mean ± S.E.M)	250mg	-	91.10 ± 9.29*	228.17 ± 1.51	25.9 ± 8.5
	500mg	-	81.70 ± 7.29*	156.33 ± 1.84	9.3 ± 8.3
Inhibition % (250mg)		-	90.68	72.17	58.8 ± 11.5
Inhibition % (500mg)		-	91.64	80.55	86.2 ± 12.2

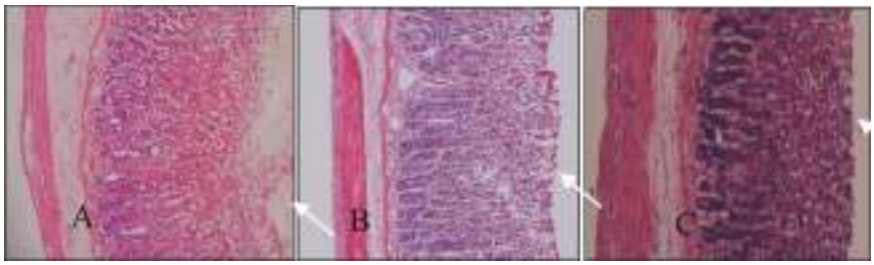

Fig. 6. Histological section of gastric mucosa in a rat pretreated with (A) 5 mL/kg of CMC (negative control), (B) 20 mg/kg of omeprazole and (C) 5 mL/kg of 500 mg/kg CXLEE (H&E stain 10x). Severe disruption at the epithelium and edema of the submucosal layer with leucocytes infiltration occurred (A). Mild disruption to the surface epithelium with mild edema and leucocytes infiltration of the submucosal layer (B) (H&E stain 10 x). White arrow represents surface epithelium and white arrow represents submucosal layer.

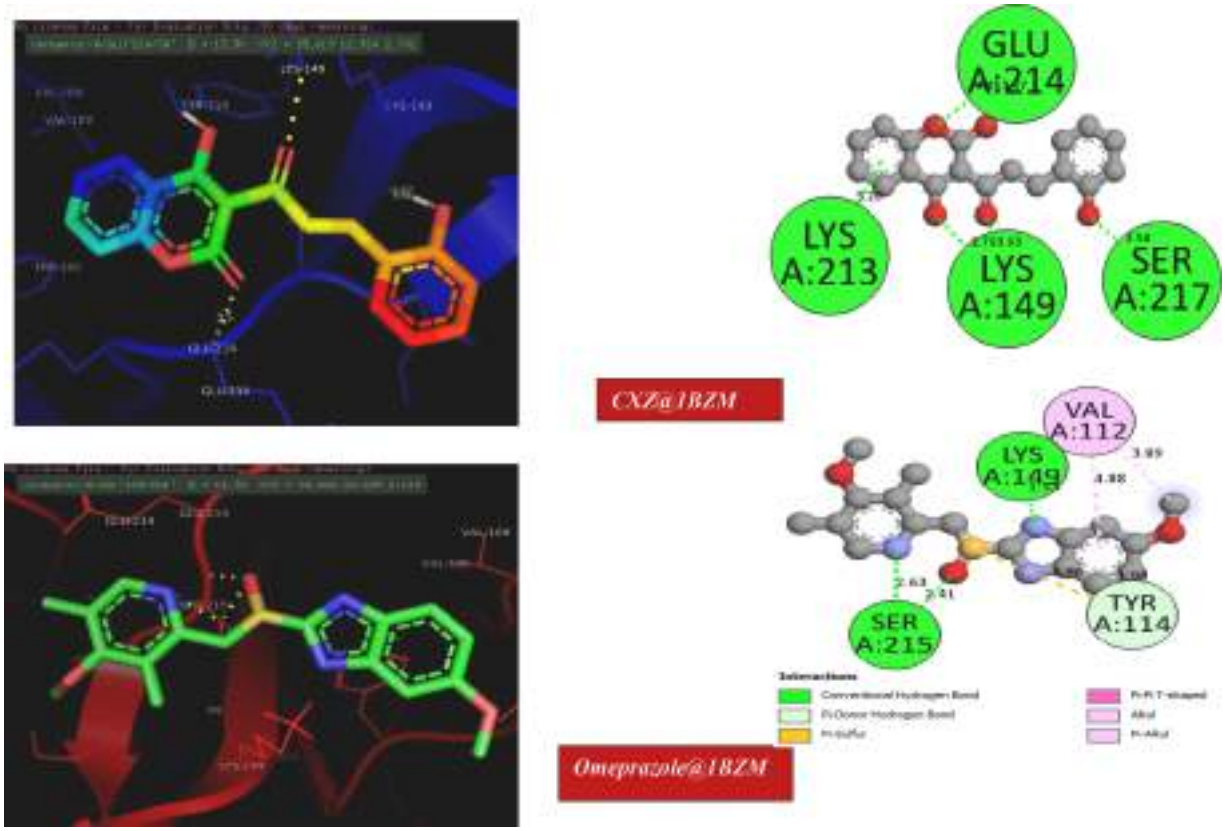

Fig. 7. 3D and 2D representation of CXZ and omeprazole docked with 1BZM.

level of theory was used to accomplish pre-geometry characterisation as well as theoretical analysis. To determine the molecular stability and chemical reactivity of the examined compounds, global descriptors at the same theoretical level were determined. Stabilization experiments were carried out to adequately assess the stability of the complex, and the results revealed that the charge delocalization from the sigma (σ) to anti-sigma (σ)*) molecular orbital was primarily responsible for the molecular stability of the investigated moleculeAccording to the estimated UV-Vis spectroscopy analysis, all absorption occurred in the visible region (400–700 nm), which is consistent with the experimentally found maximum. These findings imply that the compound under investigation may be attributed to the aromatic, amino benzoate anion, monohydrate, and oxalate moiety, respectively. According to the FMO investigations, the molecule under investigation computed a very significant energy gap of 3.437 eV, which when compared to other literature suggests that this compound has enough biological capabilities. From the natural bond analysis, it can be seen that the examined compound had the highest donor to acceptor interaction from (donor) σC20 -

C21 → σ*C28 - H30 (acceptor), σC18 - C20 → σ*C26 - C28, σC20 - H35→ *σC26 - C28 which is found to have the highest stabilization energy of 594.04 Kcal/mol. Significantly, the improved molecular structure and electronic structural analysis supported the molecular electrostatic potential (MEP) finding that the charge transfer actually occurred within the moleculeThe lead compound is evaluated as an effective phyto-compound with a better efficacy against the pharmaceutical targets based on all reports from the HOMO-LUMO, chemical reactivity, charge distribution (mulliken population analysis and MESP plots), and docking studies. As result from the topology and admet properties explicates that CXZ molecule exhibited good ADMET properties and therefore suggests its suitability as potential plant based drug.

Funding

This research was not funded by any Governmental or Non-governmental agency.

CRediT authorship contribution statement

Suhailah Wasman Qader: Project conceptualization, design, and supervision. **A. Suvitha, Mehmet Ozdemir** and **Anu Sai Ram NSA:** Writing, results extraction, analysis, and manuscript first draft. **Innocent Benjamin:** supervision, Manuscript revision, review, and proof-reading, Writing, editing, and analysis. **Martilda U. Akem, Eze Frank Ahuekwe and Emereze C. Eluwa:** Writing, editing, and analysis.

Declaration of Competing Interest

All authors declare zero financial or inter-personal conflict of interest that could have influenced the research work or results reported in this research paper.

Data availability

Data will be made available on request.

Supplementary materials

Supplementary material associated with this article can be found, in the online version, at doi:10.1016/j.chphi.2022.100130.

References

[1] A.M. Sontsa-Donhoung, M. Bahdjolbe, D. Nwaga, Selecting Endophytes for Rhizome Production, Curcumin Content, Biocontrol Potential, and Antioxidant Activities of Turmeric (Curcuma longa), Biomed Res. Int. 2022 (2022).
[2] B. Jyotirmayee, G. Mahalik, A review on selected pharmacological activities of Curcuma longa L, Int. J. Food Prop. 25 (1) (2022) 1377–1398.
[3] Klau, M. E., Rohaeti, E., Rafi, M., Artika, I. M., Ambarsari, L., & Nurcholis, W. (2022). Metabolite Profiling of Curcuma zanthorrhiza Varieties Grown in Different Regions Using UHPLC-Q-Orbitrap-HRMS and Chemometrics Analysis.
[4] S. Fuloria, J. Mehta, A. Chandel, M. Sekar, N.N.I.M. Rani, M.Y. Begum, N. K. Fuloria, A comprehensive review on the therapeutic potential of Curcuma longa Linn. in relation to its major active constituent curcumin, Front. pharmacol. 13 (2022).
[5] M.F.R. Syaban, R.F. Muhammad, B. Adnani, G.F.A. Putra, N.E. Erwan, S. D. Arviana, D.B. Kurniawan, Molecular Docking Studies of Interaction Curcumin against Beta-secretase 1, Amyloid A4 Protein, Gamma-secretase and Glycogen Synthase Kinase-3β as Target Therapy for Alzheimer Disease, Res. J. Pharm. Technol. 15 (7) (2022) 3069–3074.
[6] S.S. Panda, Q.L. Tran, P. Rajpurohit, G.G. Pillai, S.J. Thomas, A.E. Bridges, …, B. L. Lokeshwar, Design, Synthesis, and Molecular Docking Studies of Curcumin Hybrid Conjugates as Potential Therapeutics for Breast Cancer, Pharmaceuticals 15 (4) (2022) 451.
[7] M. Ahmed, M.A. Qadir, A. Hameed, M.N. Arshad, A.M. Asiri, M. Muddassar, Sulfonamides containing curcumin scaffold: Synthesis, characterization, carbonic anhydrase inhibition and molecular docking studies, Bioorganic chemistry 76 (2018) 218–227.
[8] V. Furlan, J. Konc, U. Bren, Inverse molecular docking as a novel approach to study anticarcinogenic and anti-neuroinflammatory effects of curcumin, Molecules 23 (12) (2018) 3351.
[9] M. Kumar, K.K. Sodhi, D.K. Singh, Addressing the potential role of curcumin in the prevention of COVID-19 by targeting the Nsp9 replicase protein through molecular docking, Archives of microbiology 203 (4) (2021) 1691–1696.
[10] H. Hussain, S. Ahmad, S.W.A. Shah, M. Ghias, A. Ullah, S.U. Rahman, …, S. Alghamdi, Neuroprotective Potential of Synthetic Mono-Carbonyl Curcumin Analogs Assessed by Molecular Docking Studies, Molecules 26 (23) (2021) 7168.
[11] W. Cao, X. Chen, Y. Chin, J. Zheng, P.E. Lim, C. Xue, Q. Tang, Identification of curcumin as a potential α-glucosidase and dipeptidyl-peptidase 4 inhibitor: Molecular docking study, in vitro and in vivo biological evaluation, J. Food Biochem. 46 (3) (2022) e13686.
[12] M. Govindammal, M. Prasath, S. Kamaraj, S. Muthu, M. Selvapandiyan, Exploring the molecular structure, vibrational spectroscopic, quantum chemical calculation and molecular docking studies of curcumin: A potential PI3K/AKT uptake inhibitor, Heliyon 7 (4) (2021) e06646.
[13] R. Suravajhala, A. Parashar, G. Choudhir, A. Kumar, B. Malik, V.A. Nagaraj, P. B. Kishor, Molecular docking and dynamics studies of curcumin with COVID-19 proteins, Netw. Model. Anal. Health Inform. Bioinform. 10 (1) (2021) 1–10.
[14] A. Dwivedi, A. Kumari, M. Aarthy, S.K. Singh, M. Ojha, S. Jha, N.S. Jha, Spectroscopic and molecular docking studies for the binding and interaction aspects of curcumin-cysteine conjugate and rosmarinic acid with human telomeric G-quadruplex DNA, Netw. Model. Anal. Health Inform. Bioinform. 182 (2021) 1463–1472.
[15] R. Debroy, S. Ramaiah, MurC ligase of multi-drug resistant Salmonella Typhi can be inhibited by novel Curcumin derivative: Evidence from Molecular Docking and Dynamics Simulations, Int. J. Biochem. Cell Biol. (2022), 106279.
[16] G. Moreno-Q, A. Herrera-R, A.F. Yepes, T.W. Naranjo, W. Cardona-G, Proapoptotic Effect and Molecular Docking Analysis of Curcumin–Resveratrol Hybrids in Colorectal Cancer Chemoprevention, Molecules 27 (11) (2022) 3486.
[17] N.M. O'boyle, A.L. Tenderholt, K.M. Langner, Cclib: a library for package-independent computational chemistry algorithms, J. Comput. Chem. 29 (5) (2008) 839–845.
[18] Gaussian09, R. A. (2009). 1, mj frisch, gw trucks, hb schlegel, ge scuseria, ma robb, jr cheeseman, g. Scalmani, v. Barone, b. Mennucci, ga petersson et al., gaussian. *Inc., Wallingford CT, 121*, 150-166.
[19] R. Dennington., T.A. Keith., & J. M. Millam., GaussView 6.0. 16. *Semichem Inc.: Shawnee Mission, KS, USA*. HyperChem, T. (2001). HyperChem 8.07, HyperChem Professional Program. *Gainesville, Hypercube*. (2016).
[20] Z. Parsaee, K. Mohammadi, Synthesis, characterization, nano-sized binuclear nickel complexes, DFT calculations and antibacterial evaluation of new macrocyclic Schiff base compounds, J. Mol. Struct. 1137 (2017) 512–523.
[21] O.A. El-Gammal, T.H. Rakha, H.M. Metwally, G.M. Abu El-Reash, Synthesis, characterization, DFT and biological studies of isatinpicolinohydrazone and its Zn (II), Cd(II) and Hg(II) complexes, Spectrochim. Acta A Mol. Biomol. Spectrosc. 127 (2014) (2014) 144–156.
[22] R.P. Dubey, U.H. Patel, S.B. Pandya, K.P. Chaudhary, B.N. Socha, Cadmium complex of sulfathiazole dihydrate with secondary ligand pyridine: structure, DFT studies, Hirshfeld surface analysis and antimicrobial activity, Indian J. Phys. (2019), https://doi.org/10.1007/s12648-019-01680-8.
[23] B.F. Rizwana, J.C. Prasana, C.S. Abraham, S. Muthu, Spectroscopic investigation, hirshfeld surface analysis and molecular docking studies on anti-viral drug entecavir, J. Mol. Struct. 1164 (2018) 447–458.
[24] J. Ebrahimi, M. Ghorbanzadeh Ahangari, M. Jahanshahi, Computational studies at the density functional theory (DFT) level about the surface functionalization of hexagonal monolayers by chitosan monomer, Appl. Surf. Sci. 440 (2018) 778–789.
[25] Y. Cao, A. Khan, H. Balakheyli, A.N.K. Lup, M.R. Taghartapeh, H. Mirzaei, S. R. Khandoozi, A. Soltani, M. Aghaei, F. Heidari, S.M. Sarkar, A.B. Albadarin, Penicillamine functionalized B12N12 and B12CaN12 nanocages act as potential inhibitors of proinflammatory cytokines: A combined DFT analysis, ADMET and molecular docking study, Arab. J. Chem. 14 (2021), 103200.
[26] Mahmood, A. Albo Hay Allah, Asim A. Balakit, Hamida Idan Salman, Ali Ahmed Abdulridha, and Yusuf Sert,". *New Heterocyclic Compound as Carbon Steel Corrosion Inhibitor in*, 1, 1-23.
[27] N. Dege, H. Gökce, O.E. Doğan, G. Alpaslan, T. Ağar, S. Muthu, Y. Sert, Quantum computational, spectroscopic investigations on N-(2-((2-chloro-4, 5-dicyano-phenyl) amino) ethyl)-4-methylbenzenesulfonamide by DFT/TD-DFT with different solvents, molecular docking and drug-likeness researches, Colloids Surf. A: Physicochem. Eng. Asp. 638 (2022), 128311.
[28] M. Gümüş, Ş.N. Babacan, Y. Demir, Y. Sert, İ. Koca, İ. Gülçin, Discovery of sulfadrug–pyrrole conjugates as carbonic anhydrase and acetylcholinesterase inhibitors, Archiv. Der. Pharmazie 355 (1) (2022), 2100242.
[29] I. Mahmudov, Y. Demir, Y. Sert, Y. Abdullayev, A. Sujayev, S.H. Alwasel, I. Gulcin, Synthesis and inhibition profiles of N-benzyl-and N-allyl aniline derivatives against carbonic anhydrase and acetylcholinesterase–A molecular docking study, Arab. J. Chem. 15 (3) (2022), 103645.
[30] E.A. Eno, H. Louis, P. Ekoja, I. Benjamin, S.A. Adalikwu, M.M. Orosun, E. C. Agwamba, Experimental and computational modeling of the biological activity of benzaldehyde sulphur trioxide as a potential drug for the treatment of Alzheimer disease, J. Indian Chem. Soc. 99 (7) (2022), 100532.
[31] B.K. Das, P.V. Pushyaraga, D. Chakraborty, Computational insights into factor affecting the potency of diaryl sulfone analogs as Escherichia coli dihydropteroate synthase inhibitors, Comput. Biol. Chem. 78 (2019) 37–52.
[32] I. Benjamin, A.D. Udoikono, H. Louis, E.C. Agwamba, T.O. Unimuke, A.E. Owen, A. S. Adeyinka, Antimalarial potential of naphthalene-sulfonic acid derivatives:

Molecular electronic properties, vibrational assignments, and in-silico molecular docking studies, J. Mol. Struct. (2022), 133298.
[33] E.A. Eno, J.I. Mbonu, H. Louis, F.S. Patrick-Inezi, T.E. Gber, T.O. Unimuke, O. E. Offiong, Antimicrobial activities of 1-phenyl-3-methyl-4-trichloroacetyl-pyrazolone: Experimental, DFT studies, and molecular docking investigation, J. Indian Chem. Soc. 99 (7) (2022), 100524.
[34] E.C. Agwamba, I. Benjamin, H. Louis, A.D. Udoikono, A.T. Igbalagh, T. C. Egemonye, A.S. Adeyinka, Antitubercolusic Potential of Amino-(formylphenyl) Diazenyl-Hydroxyl and Nitro-Substituted Naphthalene-Sulfonic Acid Derivatives: Experimental and Theoretical Investigations, Chemistry Africa (2022) 1–17.
[35] E.C. Agwamba, A.D. Udoikono, H. Louis, E.U. Udoh, I. Benjamin, A.T. Igbalagh, U. B. Ushaka, Synthesis, characterization, DFT studies, and molecular modeling of azo dye derivatives as potential candidate for trypanosomiasis treatment, Chem. Phys. Impact (2022), 100076.
[36] H.O. Edet, H. Louis, I. Benjamin, M. Gideon, T.O. Unimuke, S.A. Adalikwu, A. S Adeyinka, Hydrogen storage capacity of C12X12 (X= N, P, and Si), Chem. Phys. Impact (2022), 100107.
[37] E.C. Agwamba, H. Louis, I. Benjamin, C.G. Apebende, T.O. Unimuke, H.O. Edet, …, A.S. Adeyinka, (E)-2-((3-Nitrophenyl) Diazenyl)-3-Oxo-3-Phenylpropanal: Experimental, DFT Studies, and Molecular Docking Investigations, Chemistry Africa (2022) 1–17.
[38] H. Louis, D.E. Charlie, I.O. Amodu, I. Benjamin, T.E. Gber, E.C. Agwamba, A. S. Adeyinka, Probing the Reactions of Thiourea (CH4N2S) with Metals (X= Au, Hf, Hg, Ir, Os, W, Pt, and Re) Anchored on Fullerene Surfaces (C59X), ACS Omega (2022).
[39] T.E. Gber, H. Louis, A.E. Owen, B.E. Etinwa, I. Benjamin, F.C. Asogwa, …, E.A. Eno, Heteroatoms (Si, B, N, and P) doped 2D monolayer MoS 2 for NH 3 gas detection, RSC Advances 12 (40) (2022) 25992–26010.
[40] F.C. Asogwa, E.C. Agwamba, H. Louis, M.C. Muozie, I. Benjamin, T.E. Gber, A. I. Ikeuba, Structural benchmarking, density functional theory simulation, spectroscopic investigation and molecular docking of N-(1H-pyrrol-2-yl) methylene)-4-methylaniline as castration-resistant prostate cancer chemotherapeutic agent, Chem. Phys. Impact 5 (2022), 100091.
[41] E.C. Agwamba, A.D. Udoikono, H. Louis, E.U. Udoh, I. Benjamin, A.T. Igbalagh, …, U.B. Ushaka, Synthesis, characterization, DFT studies, and molecular modeling of azo dye derivatives as potential candidate for trypanosomiasis treatment, Chemical Physics Impact (2022), 100077.
[42] B.E. Inah, L. Hitler, B. Innocent, T. Unimuke, A.S. Adeyinka, Computational study on the interactions of functionalized C24NC (NC= C,-OH,-NH2,–COOH, and B) with chloroethylphenylbutanoic acid, Can. J. Chem. (2022).
[43] J.G. Hill, A.C. Legon, Radial Potential Energy Functions of Linear Halogen-Bonded Complexes YX··· ClF (YX= FB, OC, SC, N2) and the Effects of Substituting X by Second-Row Analogues: Mulliken Inner and Outer Complexes, J. Phys. Chem. A 126 (16) (2022) 2511–2521.
[44] G. Golding Sheeba, D. Usha, M. Amalanathan, M. Sony Michael Mary, H. MarshanRobert, Molecular structure, vibrational spectroscopic, frontier molecular orbital and natural bond orbital analysis of anti-cancer drug 6-chloro-3-pyridine carbonitrile, Spectrosc. Lett. 54 (6) (2021) 419–436.
[45] M. Fizer, O. Fizer, Theoretical study on charge distribution in cetylpyridinium cationic surfactant, J. Mol. Model. 27 (7) (2021) 1–11.
[46] M.A.A. Tayeb, N. Tchouar, F.A. Miannay, A. Idrissi, Effect of the mixture composition of C4mimBF4/acetonitrile on the charge transfer in Coumarin 153: DFT and TD-DFT analysis, J. Mol. Liq. 339 (2021), 116830.
[47] M.A.M. El-Mansy, A. Suvitha, B. Narayana, Exploring crystal, electronic, optical and NLO properties of ethyl 4-(3, 4-dimethoxy phenyl)-6-methyl-2-thioxo-1, 2, 3, 4-tetrahydro pyrimidine-5-carboxylate (MTTHPC), Opt. Quantum Electron 53 (8) (2021) 1–16.
[48] M.D. Mohammadi, H.Y. Abdullah, A. Suvitha, The adsorption of 1-chloro-1, 2, 2, 2-tetrafluoroethane onto the pristine, Al-, and Ga-doped boron nitride nanosheet, Iran J. Sci. Technol. Trans. A Sci. 45 (4) (2021) 1287–1300.
[49] D.E. Pires, T.L. Blundell, D.B. Ascher, pkCSM: predicting small-molecule pharmacokinetic and toxicity properties using graph-based signatures, J. Med. Chem. 58 (9) (2015) 4066–4072.
[50] A. Daina, O. Michielin, V. Zoete, SwissADME: a free web tool to evaluate pharmacokinetics, drug-likeness and medicinal chemistry friendliness of small molecules, Scientific reports 7 (1) (2017) 1–13.
[51] S. Chakravarty, K.K. Kannan, Drug-protein interactions: refined structures of three sulfonamide drug complexes of human carbonic anhydrase I enzyme, J. Mol. Biol. 243 (2) (1994) 298–309.
[52] P.P. Venugopal, B.K. Das, E. Soorya, D. Chakraborty, Effect of hydrophobic and hydrogen bonding interactions on the potency of ß-alanine analogs of G-protein coupled glucagon receptor inhibitors, Proteins: Struct. Funct. Genet. 88 (2) (2020) 327–344.

Functional Foods and Viral Diseases

First Edition, Volume 8

Functional Food Center Inc. / Functional Food Institute
5050 Quorum Drive, Suite 700, Dallas, Texas, 75254, USA
Website: http://www.functionalfoodscenter.net

Printed and Edited in the United States of America

ISBN: 979-8675209637 (Color Interior)

For information regarding special discounts for bulk purchases, please contact Food Science Publisher Special Sales at 469-441-8272 or email ffc@functionalfoodscenter.net

Important Notice:
This publication is neither a medical guide nor a manual for self-treatment. If you should suspect that you suffer from a medical problem, you should seek competent medical care. The reader should consult his or her health professional before adopting any of the suggestions in this book. Never disregard professional medical advice due to something you read in this textbook. This book only offers important information on functional foods and nutrition in overall health and wellness. Nonetheless, readers should be aware that nutrition and medicine are expanding fields and should continue to educate themselves on preventative measures. Their primary care provider and the patient are responsible for determining the best plan of care. The authors, editors, and publisher take no liability for any injury or illness that may arise by using the materials from this text.

Food Science Publisher 2020
Edited by Danik M. Martirosyan, PhD

Contents

Chapter 4

A Computational Effort to Deciphering Putative COVID-19 3C-like Protease Binders in the Selected Recipes of Kurdish Ethnomedicine: An Approach to Find an Antiviral Functional Tea

Halgurd Nadhim Mohammed[1], Layth Jasim Mohammed[2], Isaac Karimi*[2], A Suvitha[3]

[1]Pharmacy Department, Aynda Private Technical Institute, ERBIL, Iraq; [2]Department of Biology, Faculty of Science, Razi University 67149-67346, Kermanshah, Iran; [3]Department of Physics, CMR Institute of Technology, Bangalore, Karnataka, India

Corresponding author: Dr. Isaac Karimi; Department of Biology, Faculty of Science, Razi University, Kermanshah, Iran

Key words: Functional Tea, COVID-19, Protease Binders, Ethnomedicine, SARS-CoV-2 Protease

INTRODUCTION

Paleoanthropological expedition of the Shanidar cave, Zagros Mountains of Kurdistan, Iraq *shed* the *light* of truth and *knowledge* upon applications of herbal medicine through millennia [1, 2]. Ancient Kurdish used herbs for alleviating or suppressing fever. Some of the herbs used for thermoregulation in the Kurdish area are discussed here (*vide infra*).

In 2020, the World Health Organization (WHO) states that the SARS-CoV-2 coronavirus of the coronaviridae family causes novel coronavirus type 2 induced disease (COVID-19) and should be considered a pandemic disease. Since there was not an available vaccine based on results from clinical trials against this novel disease in the market, clinicians tried implementing the usual protocol of acute respiratory distress syndrome (ARDS) and, through risky drug repurposing and using an array of antiviral drugs, they want to limit virus proliferation and its shedding. Parallel to these therapeutic strategies, some computational bioscientists tried to blind screen available databases of known chemicals to discover new agents and some of these groups were lucky to be submitted to experimental and clinical trials regarding their discovered chemicals or repurposed drugs. Seminal papers [3, 4] have categorized protein targets for possible antiviral drugs or binders, amongst these papers the main SARS-CoV-2 protease (3CLpro, also known as 3-chymotrypsin-like protease) would be a canonical enzyme target and plays cardinal functions in the self-build process of coronavirus [5]. The 3CLpro known as Nsp5 (nonstructural protein 5) is initially self-cleaved from structural viral polyproteins to produce a bunch of intermediate enzymes and is finally released as Nsp4–Nsp16 for virus proliferation. Therefore, 3CLpro has been appreciated as a striking target for anti-SARS-CoV-2 drugs. In this essence, small molecules and therapeutic recombinant peptides are major compounds targeted

at druggable SARS-CoV 3CLpro until now. The 3CLpro monomer has domain I (residues 8–101), domain II (residues 102–184), domain III (residues 201–306 in α-helices) and a long loop (residues 185–200) which joins domain II and III. The torus of domain I and II primarily consists of β-barrels constructs at the active site of 3CLpro presented as uncharged Cys-His catalytic dyad (Cys145 and His41) [5, 6].

In parallel to many scientists in the world, we hypothesized that ARDS might have occurred in the history of Kurdish people settled down in Zagros mountains during millennia. We searched for Kurdish ethnomedicine books but, unfortunately, this ancient and valuable heritage has been rotted or looted due to an array of reasons not suitable to discuss here. In addition, since fever is a cardinal sign of ARDS, we hypothesized that antipyretic and anti-flu remedies used in traditional Kurdish ethnomedicine might possess antiviral effects in orthodox medicine. Based on these hypotheses, our team interviewed all traditional healers that are currently known in Erbil, Iraq (36.2^{o}N, 44.0^{o}E and 420 MASL) we recorded data and, finally, selected some plants for computational drug discovery (*vide infra*).

Antipyretic and Anti-flu Remedies Used in Kurdish Ethnomedicine

Fenugreek (*Trigonella foenum-graecum*) is one of the most famous herbal medicines that has been traditionally used in medicine and the food industry [7]. Fenugreek is a multi-effective herb known for its anticancer, antifungal, antibacterial and antiviral effects [8]. Fenugreek is the oldest medicinally used plant originating from India, north of Africa, the Kurdistan region of Iraq and Iran [9, 10]. It has been acknowledged as an antioxidative, antibacterial and antiviral remedy and can even be used for gynecological problems [11]. Fenugreek is an impressive source for the production of raw materials for the pharmaceutical industry like steroid hormones, antipyretics, and antibacterial and antiviral agents [12-14]. Likewise, it has been utilized in making sifting face covers. The current manufacture is to forestall or diminish the transmission of microbial (zoonotic) pathogens by the means of different entrances like salivation, nasal liquid or inward breath. Since the virus or microorganism inflicting such infections is often found in aerosolized media, such as excreta ejected throughout sneezing or respiratory or coughing, wearing a mask over the mouth and/or nose can be an effective approach for preventing or decreasing the transmission of sickness inflicting pathogens or viruses. However, the pores in a mask may be larger than the virus or microorganism leading to a confined utility as well as the opportunity of transmission open, despite providing a crude shielding barrier [15, 16]. Phytochemicals reported in fenugreek include flavonoids, diosgenin, alkaloids, steroids, amino acids, polyphenol compounds (e.g., rhaponticin and isovitexin), vitamin C, vitamin A, and minerals (zinc, iron, and phosphorus) [10, 11, 17, 18; Figure 1, Table 1].

Chamomile (*Matricaria chamomilla* L.), or Asteraceae, is one of the most popular herbal medicine that utilized by Kurdish people through millennia. It has been utilized by both Kurdish and Iranian people since it is a spice local to southern and eastern Europe. Chamomile blossoms has been applied to treat fever and contaminations for many years [19, 20]. Phytochemicals found in chamomile flowers include sesquiterpenes, *β*-farnesene, coumarins, flavonoids, phenolic acid, and various glucosides. The dried flowers and essential oils extracted from chamomile have been considered as therapeutics, functional ingredients or herbal teas [20-22; Figure 1, Table 1]. The antiviral effects of various formulations of chamomile against viruses that attack the human respiratory system such as the common cold and the influenza virus has been reported [20, 22, 23]. The formulations of chamomile which are affluent with *β*-farnesene, flavonoids, bisabolol oxid, matricin, chamazulene, umbelliferone, and chlorogenic acid can potentiate the immune system against viruses, especially respiratory viruses [20, 22, 23].

Salvia officinalis, or Labiatae/Lamiaceae, is usually known as **sage**, kitchen sage, Dalmatian sage, golden sage, garden sage, and maramia in the east. Nowadays, *Salvia* has been adopted globally, although it is a native plant to the Mediterranean area. *Saliva* species have been employed traditionally for a set of common problems including pain, fever, oxidative stress, angiogenesis, and inflammation while it also possesses antibacterial and antiviral effects [24, 25]. *Salvia* is popularly used to treat infection, cough, and

mouth and throat inflammations. The *Salvia* oil remedy is a source of anticancer and antioxidative phytocompounds that prove to be useful against diseases of the respiratory system and the oil can also control proliferation of human cells [26-28].

Famous phytocompounds of *salvia* include phenolics, polyphenols, terpenes, and flavonoids [29]. In this essence, ursolic acid as a pentacyclic triterpenoid has strong anti-inflammatory properties, while hydroalcoholic extracts derived from salvia contain polyphenols, terpenes, and flavonoids that inhibit bacteria and viruses [25, 30; Figure 1, Table 1]. The pharmacological properties of salvia-based formulations as anticancer, antiviral, antibacterial, antiseptic, antioxidative and anti-inflammatory agents have been supported by both experimental and clinical research [29, 31, 32].

Ginger (*Zingiber officinale* Roscoe), also called Zingiberaceae, is dubbed for its application as a pungent, fragrant spice in the culinary system. This spice is constituted of the chipped or ground rhizome (underground stem) of the plant. Ginger is a natural pharmacy of antispasmodic, antistomachic, vasodilator, expectorant, bronchodilator, analgesic, and antitussive functional formulations in the hands of traditional healers for treating pulmonary diseases. Ginger modulates the inflammatory cytokines to counterbalance pro-inflammatory and anti-inflammatory ones [33] and, more specifically, ginger consists of very effective anti-inflammatory compounds known as gingerols [34, 35; Figure 1, Table 1]. Ginger is a rich wellspring of nutrients such as vitamins (C, E, B3, B5, and B6), *β*-sesquiphellandrene, flavonoid, camphene, sabinene, pinocarvone, and borneol. Ginger can diminish chemotherapy-induced nausea and can provide some protection towards cancer cells. In essence, ginger is dubbed as the golden phytomedicine prescribed in cancer therapy [28, 36-38]. Ginger is highly effective against the respiratory syncytial virus, the influenza A virus subtype H1N1, and the common influenza virus and is a treasure to be deciphered for its antiviral agents to treat ARDS [36, 39, 40].

Figure 1. Putative anti-COVID-19 plants selected from Kurdish ethnomedicine (Erbil, Iraq); a: Fenugreek (*Trigonella foenum-graecum*); b: Chamomile (*Matricaria chamomilla* L.); c: Sage (*Salvia officinalis*); d: Ginger (*Zingiber Officinale*)

Table 1. Selected therapeutic phytocompounds of putative anti-COVID-19 plants used in Kurdish ethno-medicine (Erbil, Iraq)

A. Fenugreek *(Trigonella foenum-graecum*)

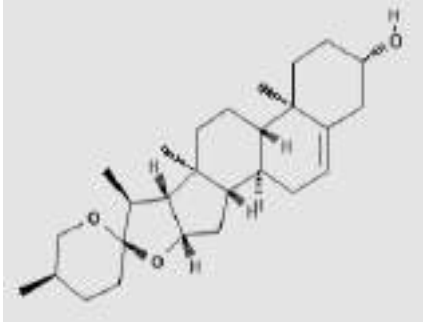

Diosgenin

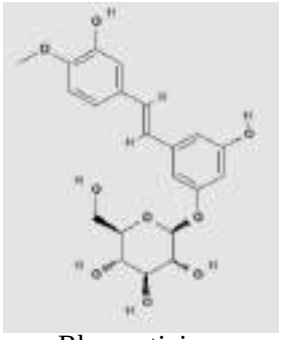

Rhaponticin

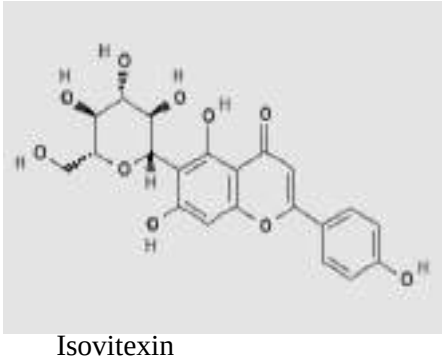

Isovitexin

B. Chamomile (*Matricaria chamomilla* L.)

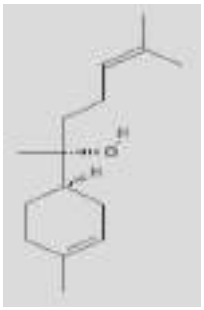

(-)-α-bisabolol

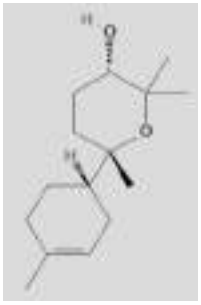

Bisabolol oxide

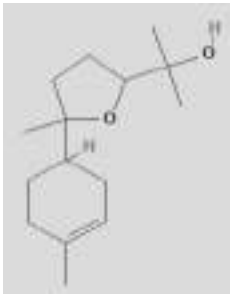

Bisabolol oxide B

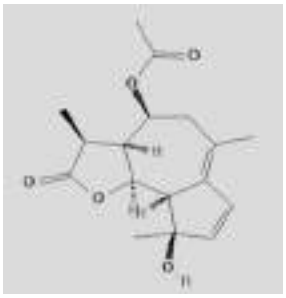

Matricin

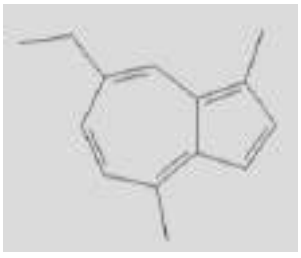

Chamazulene

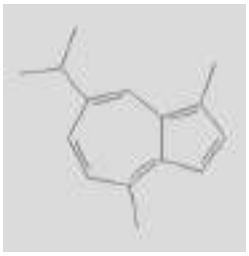

Guaiazulene

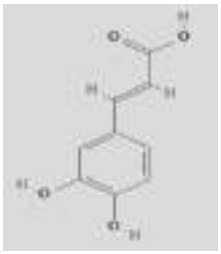

Caffeic acid

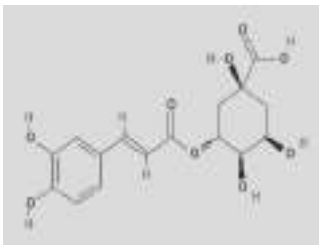

Chlorogenic acid

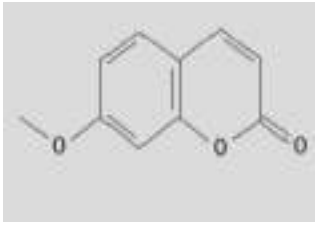

Herniarin

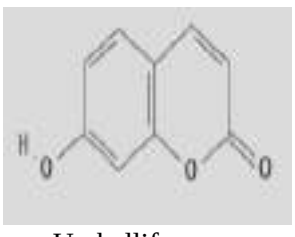

Umbelliferone

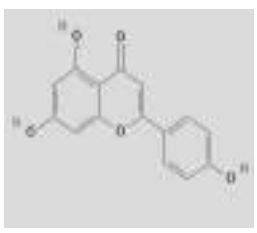

Apigenin

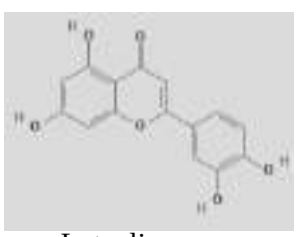

Luteolin

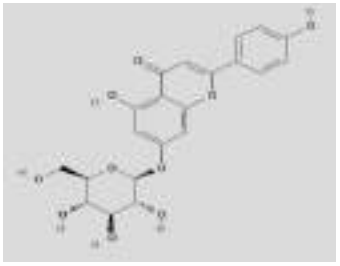

Apigenin-7-*O*-glucoside

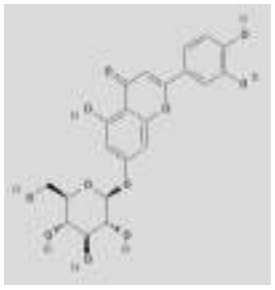

Luteolin-7-*O*-glucoside

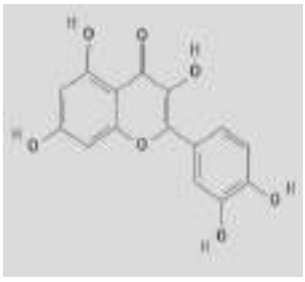

Quercetin

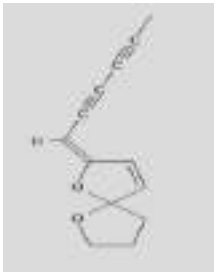

Enyne dicycloether

C. Sage (*Salvia officinalis*)

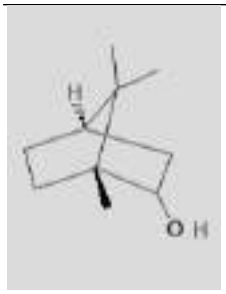

Borneol

Camphor

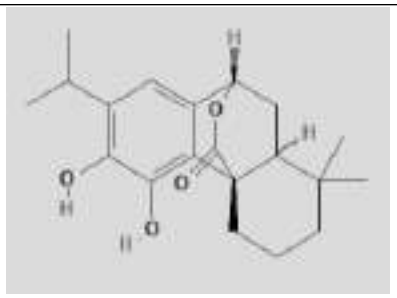

Carnosol

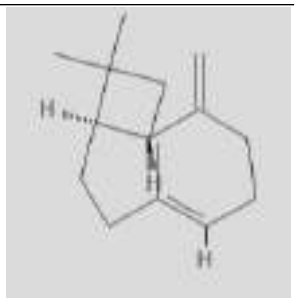

Caryophyllene

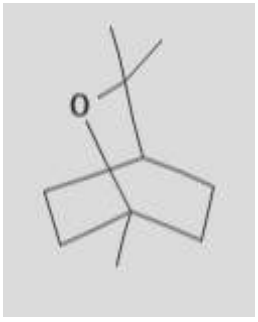

Cineole

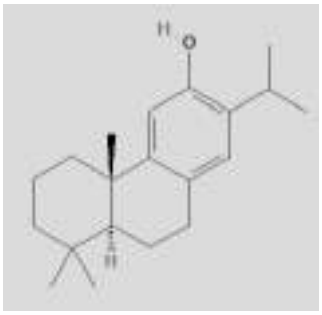

Ferruginol

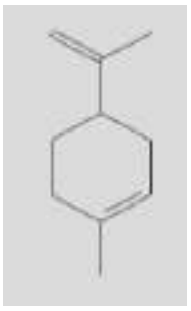

Limonene

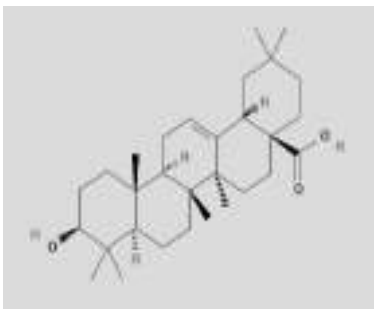

Oleanolic acid

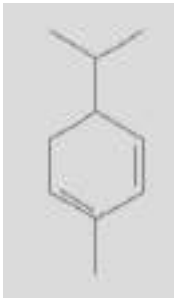

Phellandrene

Sabinene

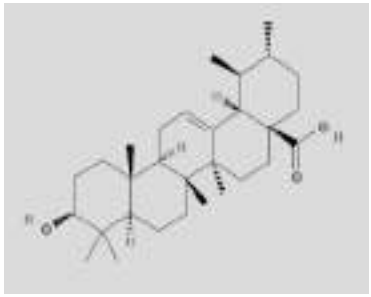

Ursolic acid

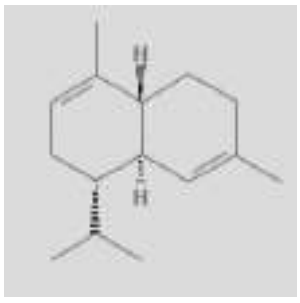

Alpha-cadinene

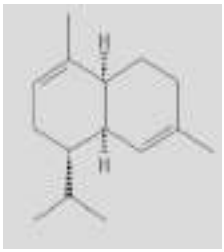
Alpha-muurolene


Alpha-pinene

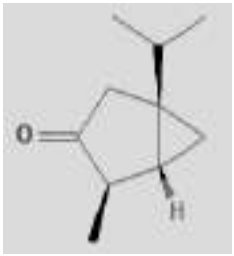

Alpha-thujone

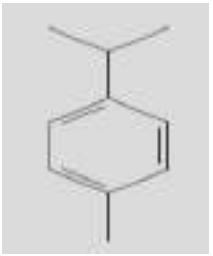
p-Cymene

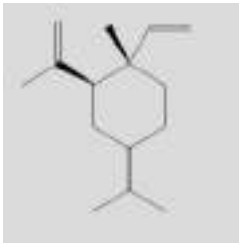
Gama-elemen

D. Ginger (*Zingiber Officinale*)


α-Thujene

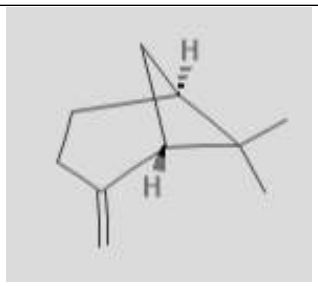

α-Pinene

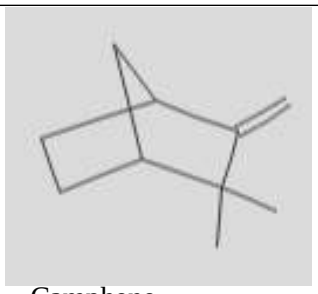
Camphene

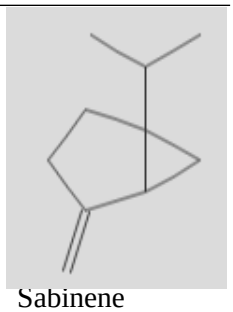
Sabinene

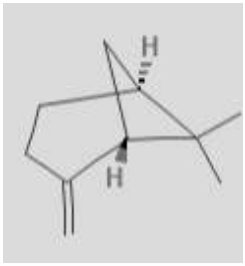

ß-Pinene

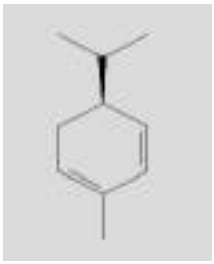
α-Phellandrene

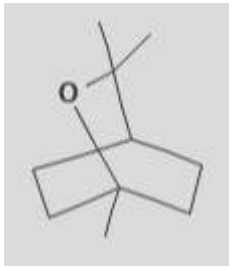

1,8-Cineole

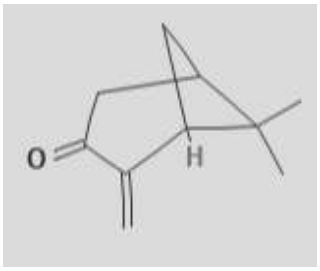

Pinocarvone

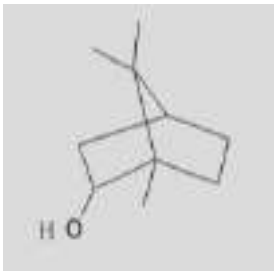

Borneol

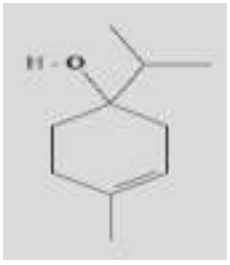

Terpinen-4-ol

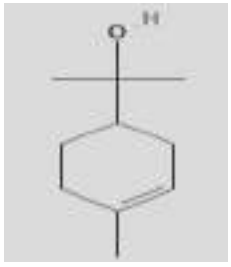

α-Terpineol

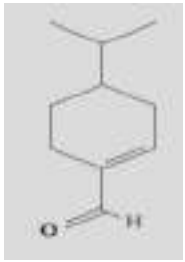

Phellandral

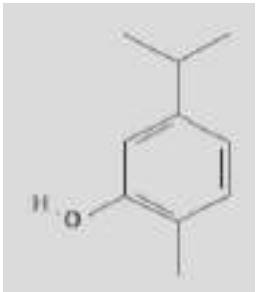

Carvacrol

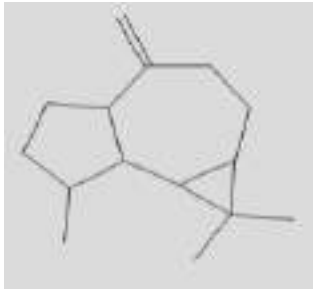
Aromadendrene

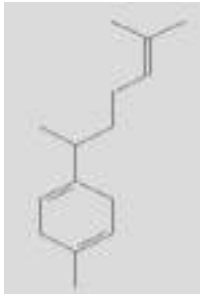
β-Curcumene

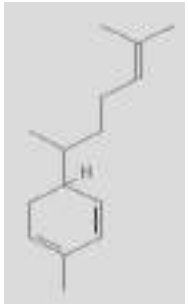

α-Zingiberene

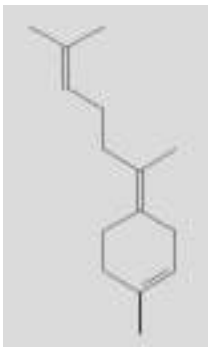

(E)-γ-Bisabolene

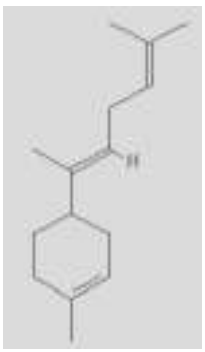

(E)-α-Bisabolene

Camphor

Computational Antiviral Assay

Computational molecular docking of the aforementioned phytocompounds (*vide supra*) and the druggable protein 6Y84 was accomplished by VINA WIZARD module introduced on PyRx programming adaptation 0.8 [41]. In this sense, the PDB format of 6Y84 was recovered from the Research Collaboratory for Structural Bioinformatics (http://www.RCSB.org) and was cut, advanced, and prepared utilizing Molegro Virtual Docker [42] and Chimera 1.8.1 (http://www.rbvi.ucsf.edu/chimera) programming projects before attempting PyRx programming. The structures of the major phytocompounds were reaped from the PubChem database (https://pubchem.ncbi.nlm.nih.gov/). The results of sub-atomic docking have been expressed as a binding affinity (BA; kcal/mol) of a set of molecular poses. The best posture of ligand, phytocompound, in counter to the target protein, prompts the most negative BA and is revealed here (*vide infra*). The best pose and 6Y84 were combined using Chimera 1.8.1 (http://www.rbvi.ucsf.edu/chimera) or Molegro Virtual Docker [42] and their graphical interface were inspected with LigPlot $^{+}$ programming to recognize amino acid deposits that engaged with bindings [43]. Conventionally, the binders, phytocompounds, which demonstrated BA lesser than -7.0 kcal/mol were discussed here.

Pharmaco- and Toxico-Kinetic Parameters

Physico-chemical properties and the computational aspects of absorption, distribution, metabolism, excretion, and toxicity (ADMET) were completed utilizing Swiss ADME programming recreation [SwissADME;http://www.swissadme.ch/] and online ADMET indicator instrument [http://biosig.unimelb.edu.au/pkcsm/prediction]. ADMET Predictor is a product instrument that rapidly and precisely predicts more than 140 properties including dissolvability, log P, pKa, locales of cytochrome P450 (CYP) digestion, and Ames mutagenicity. The program has an instinctive UI that permits one to handily control and picture information for selected compounds. In light of ADMET results, carnosol fits consummately inside the characterized boundaries for non-infringement of Lipinski's standard. A particle's log P is comprised of the expansion of its molecules. The impact of hydrogen holding onto the log P is viewed when there is a chance of shaping a six-membered ring between proper contributor and acceptor particles [44]. The molecules have log P esteems running from 0.05 to 5.18 which infers that these can successfully have reasonable cell membrane penetrability. Moreover, certain boundaries including blood-brain barrier

(BBB) infiltration, P-glycoprotein hindrance, human gastrointestinal tract assimilation, volume appropriation, subcellular limitation, CYP substrate or inhibitor, and human *ether-a-go-go-related gene* (HERG) inhibition reflect the fitness of any compound to be categorized as lead- or drug-like [45].

DISCUSSION

Fenugreek is referred to as Alhulba in Mesopotamia, Shemlia in Kurdish and Shanbalila in Persian and is used in Kurdish ethnomedicine. The Kurdish recipe for fenugreek is comprised of one big spoon of fenugreek seed boiled in hot water. It has been prescribed to drink fenugreek tea twice per day or to add a small spoon of fenugreek powder to a tablespoon of honey. Three phytocompounds of fenugreek showed acceptable BA with 3CLpro (PDB:6Y84). In this context, **diosgenin** interacted hydrophobically with a bunch of amino acid residues of all domains of 3CLpro and also used hydrogen bonds between diosgenin and Asp295 residues of 3CLpro (Figure 2). Diosgenin, a phytosteroid sapogenin, is spirostan found in Dioscorea (wild yam) species with the potential to be considered as the starting point for the commercial synthesis of a number of steroids. It plays roles as an apoptosis inducer, an antiviral agent, an antineoplastic agent and a metabolite [46]. A pivotal review [47] emphasized the pharmacology (e.g., antiviral effect) of diosgenin [48]. Based on ADMET criteria, it will not be considered as a drug-like compound (see supplementary file).

Rhaponticin displayed an array of hydrophobic interactions with 3CLpro and also employed hydrogen bonds with Met6, Val303 and Tyr154 residues of domain II and III of 3CLpro. *Rhaponticin* is a stilbenoid glucoside compound and its aglycone is called rhapontigenin [46]. A seminal review was written for the pharmacological effects of rhaponticin [49] with special appreciation to its anti-inflammatory compound. Based on the ADMET results, rhaponticin has a low water solubility which limits its pharmacological applications in pristine form (see supplementary file).

Isovitexin hydrophobically interacted with a bunch of amino acid residues of 3CLpro and also employed hydrogen bonds with the Ala7 residues of 3CLpro. Isovitexin (6-*C*-glucosylapigenin) is an alpha-glucosidase (EC 3.2.1.20) inhibitor [46]. Isovitexin was considered to donate antiviral and anti-inflammatory effects via the inhibition of cyclooxygenase-2 mRNA expression [50].

Table 2. Computational binding affinities of major phytochemicals of *Trigonella foenum-graecum* with protease (PDB code 6Y84) of coronavirus

Ligand of PubChem; ID)	Binding affinity (Kcal/mol)	RMSD/UB	RMSD/LB
Diosgenin 99474	-8.9	2.77	1.045
Rhaponticin 637213	-8.3	2.442	1.474
Isovitexin 162350	-7.6	3.75	2.615

Note: RMSD: root mean-square deviation is the normal separation between the particles. UB: upper bound; LB: lower bound.

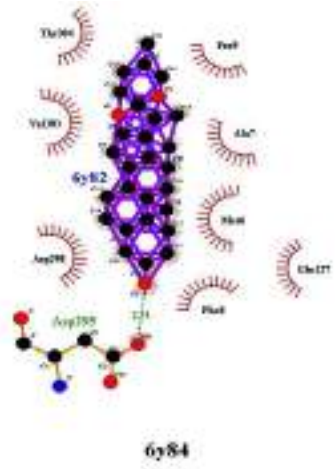

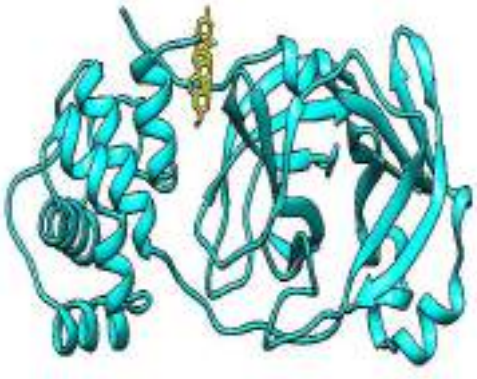

6Y84-Diosgenin

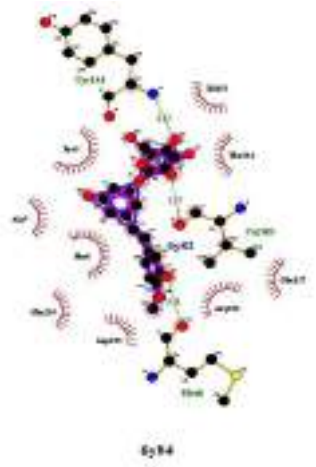

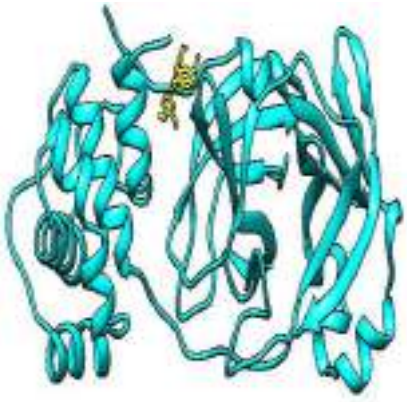

6Y84-Rhaponticin

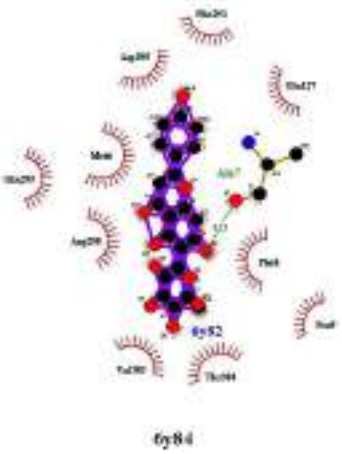

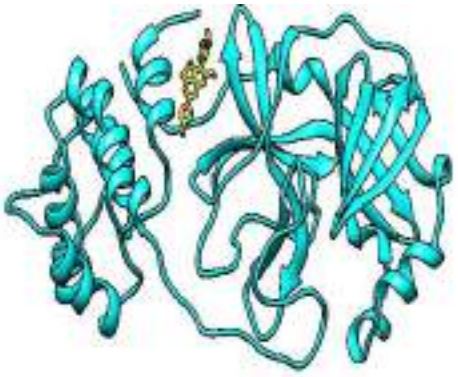

6Y84-Isovitexin

Figure 2. Molecular docking of phytocompounds of *Trigonella foenum-graecum* (in yellow shading) with protease (PDB code 6Y84) of *coronavirus*; in cyan shading). Hydrogen bonds are highlighted by dashed lines, while hydrophobic interactions are represented by an arc.

Chamomile is known as Albabunaj in Mesopotamia, Chawa Peshila in Kurdish and Babunah in Persian. A hot drink of chamomile is one of the oldest known folk remedies because of its many health promoting properties. Chamomile is prescribed as a suspension of one tablespoon of orange juice to a cup of hot chamomile tea, or as a mixture of small spoon of ginger powder and a cup of chamomile hot tea. Based on the *in-silico* findings, phytocompounds reported in chamomile showed reliable BAs with 3CLpro with this order: chlorogenic acid < luteolin-7-*O*-glucoside < apigenin-7-*O*-glucoside < quercetin < luteolin < matricin < caffeic acid (Table 3). In this continuum, luteolin-7-*O*-glucoside, cynaroside flavone, and chlorogenic acid with the best BAs amongst chamomile derived phytocompounds interacted hydrophobically with 3CLpro and also employed hydrogen bonds with 3CLpro (Figure 3). Luteolin 7-glucoside is found in various plants including *Capsicum annuum* (red pepper), *Ferula varia*, *F. foetida*, dandelion coffee, *Campanula persicifolia*, Campanula *rotundifolia*, and *Cynara scolymus* (artichoke) [46]. More specifically, **luteolin-7-*O*-glucoside** was recognized as a functional antiviral and antioxidative constituent of the lettuce (*Lactuca sativa* L.) extracts [51]. The poor water solubility of luteolin-7-*O*-glucoside is a principal factor in restricting further investigations on its pharmacological activities and new innovation of medication conveyance is mentioned to expand its bioavailability, however, it is not the substrate or inhibitor of CYP isoenzymes which mediate xenobiotic metabolism (see supplementary file). **Luteolin**, a flavonoid, is named as a fundamental phytomedicine of the human eating routine [46] and is used in hydrophobic interactions and hydrogen bonds with Asp295, Met6 and Gln299 residues of 3CLpro with considerable looser BA in comparison to its conjugated form, luteolin-7-*O*-glucoside (Figure 3). It has been reported that luteolin is a potent antiviral bioflavonoid utilized against Japanese encephalitis virus replication [52]. Based on ADMET results, lutein showed better results in comparison to its glycosidic conjugate, luteolin-7-*O*-glucoside, however, it interacts with CYP isoenzymes (see supplementary file).

Apigenin-7-*O*-glucoside, a glycosyloxyflavone, showed hydrophobic interactions and hydrogen bonds with the loop of 3CLpro (Figure 3). This conjugated flavonoid compound, like its other congeners, possesses various antiviral effects (see a review [53]). Apigenin-7-*O*-glucoside demonstrated low water solubility, suitable metabolism, and three violations against Lipinski's rule (see supplementary file).

Chlorogenic acid, an ester of quinic acid and caffeic acid [46], hydrophobically interacted with an array of amino acid residues in domain I and III of 3CLpro. It also employed a set of hydrogen bonds to interact with loop and domains of 3CLpro (Figure 3). Chlorogenic acid is known as the major polyphenolic compound in coffee and is usually isolated from dicotyledonous plants [46]. This caffeoylquinic acid moiety, known as an antioxidative and cardioprotective component, may affect COVID-19-induced cardiovascular disorder. *Lonicera japonica* Thunb, is a rich wellspring of chlorogenic acid endorsed in customary Chinese medication to treat upper respiratory tract infections like the flu, parainfluenza, and respiratory syncytial infection. Additionally, it is also known as a neuraminidase blocker of influenza A virus [54]. Chlorogenic acid showed two violations against Lipinski's rule due to low water solubility and the number of hydrogen donor atoms and new portal like liposome that is needed to reach the cytoplasm (see supplementary file).

Matricin, a sesquiterpene lactone, has interacted hydrophobically with domain I and III and via hydrogen bonds with Asp295 residue of the loop of 3CLpro (Figure 3). This natural profen has various pharmacological effects like anti-flu activities and has been considered to be a prodrug [55]. Matricin showed suitable ADMET results, however, it has low water solubility and volume distribution in addition to some kinds of toxicity (see supplementary file).

Caffeic acid, a catechol of hydroxycinnamic acid derivative and polyphenol, hydrophobically interacted with domain II and III of 3CLpro and also employed hydrogen bonds with Asp295 residue in domain III of 3CLpro (Figure 3). Caffeic acid possesses antioxidative, anti-inflammatory, enzyme inhibitory, and

antineoplastic activities [46]. The antiviral potential of caffeic acid has been accounted for in flu [56] and severe fever with thrombocytopenia syndrome virus [57]. Caffeic acid has been shown to have good intestinal absorption as well as suitable ADMET results (see supplementary file).

Quercetin has interacted with all domains of 3CLpro through hydrophobic interactions and hydrogen bonding with the Asp295 residue of domain III (Figure 3). Quercetin is a glycan polyphenolic flavonoid found ubiquitously in fruits and vegetables with special immunomodulatory [58] and antiviral activity against influenza A virus **[**59]. The number of hydrogen donor atoms of quercetin exceed 5 and, thus, violates Lipinski's rule (see supplementary file). The water solubility and intestinal absorption of quercetin also are not suitable for consideration it as a drug-like compound, however, quercetin may interfere with virus entry to cells **[**59].

Table 3. Computational binding affinities of major phytochemicals of *Matricaria chamomilla* L. with protease (PDB code 6Y84) of coronavirus

Ligand of PubChem; ID)	Binding affinity (Kcal/mol)	RMSD/UB	RMSD/LB
Matricin 92265	-7.1	3.903	2.024
Caffeic acid 689043	-7.0	3.078	2.445
Chlorogenic acid 1794427	-9.2	2.067	1.380
Luteolin 5280445	-7.9	30.743	27.341
Apigenin-7-*O*-glucoside 5280704	-8.9	2.58	1.269
Luteolin-7-*O*-glucoside 5280637	-9.1	29.959	25.778
Quercetin 5280343	-8.1	1.887	1.364

Note: RMSD: root mean-square deviation is the average distance between the atoms. UB: upper bound; LB: lower bound.

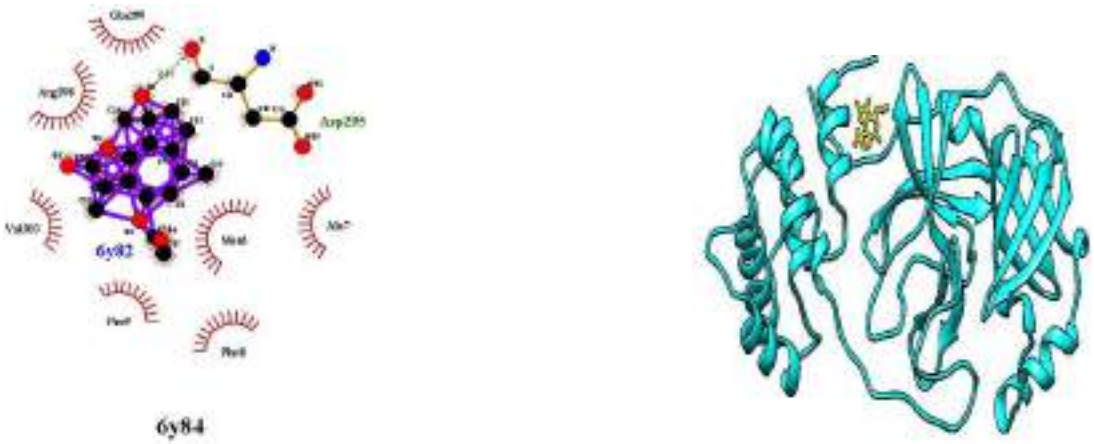

6Y84-Matricin

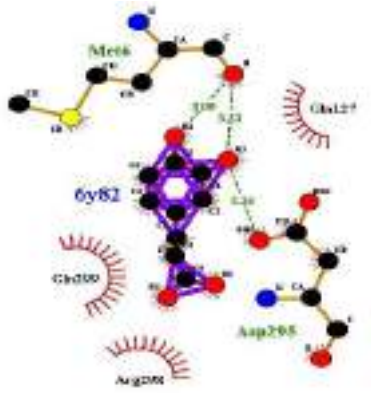

6y84

6Y84-Caffeic acid

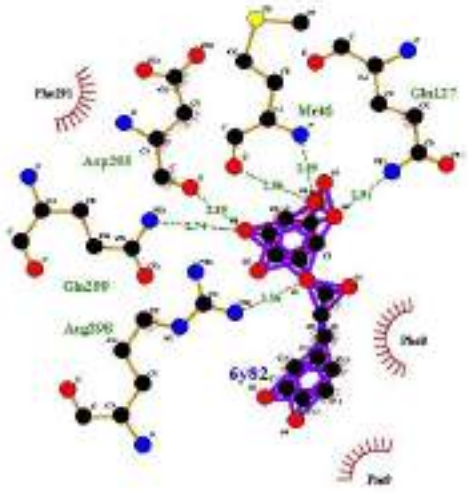

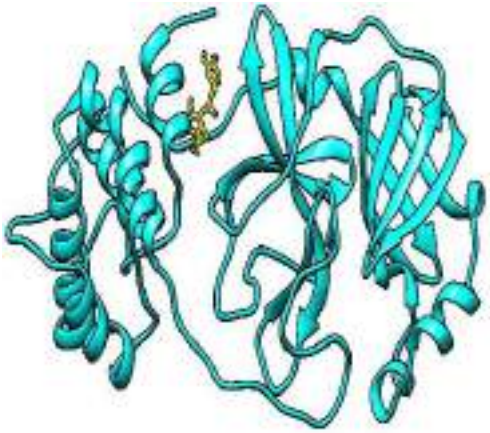

6y84

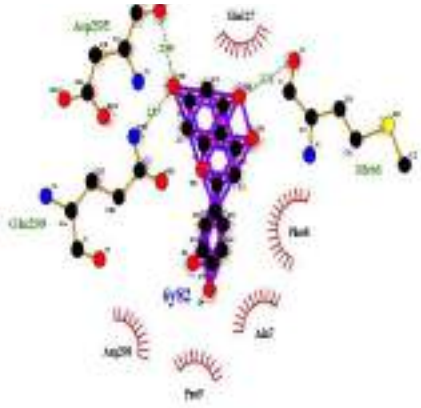

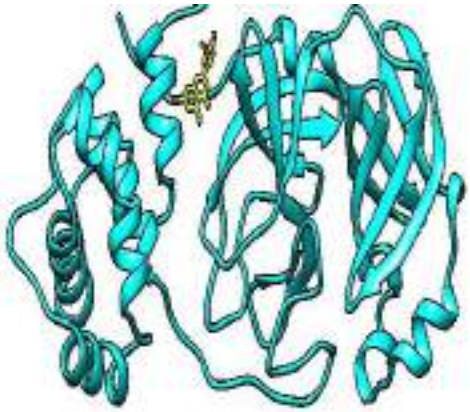

6y84

6Y84-Luteolin

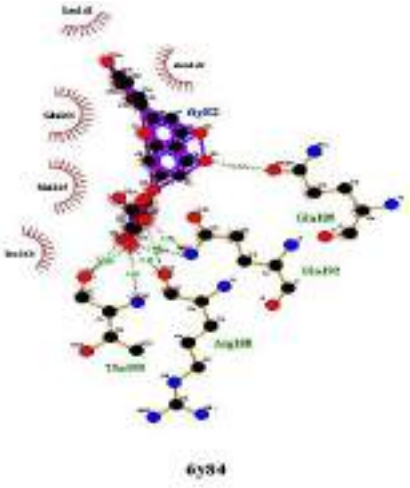

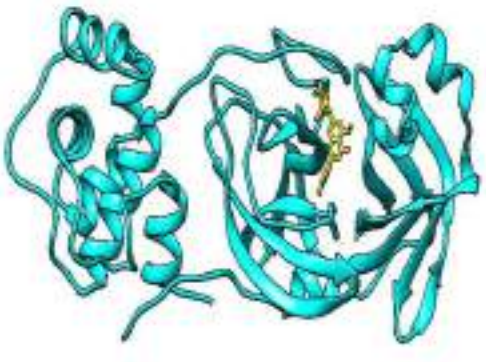

6Y84-Apigenin-7-*O*-glucoside

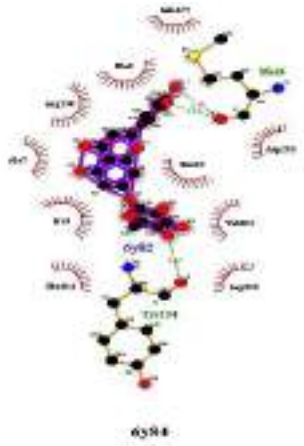

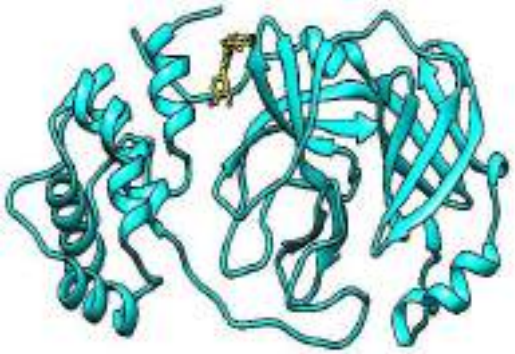

6Y84-Luteolin-7-*O*-glucoside

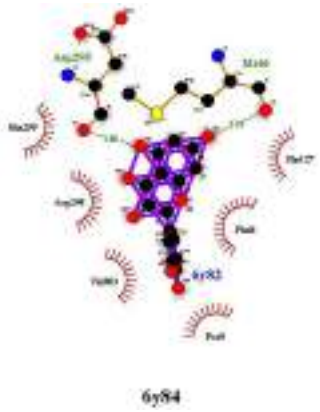

6Y84-Quercetin

Figure 3. Molecular docking of phytochemicals of *Matricaria chamomilla* L. (in yellow shading) against protease (PDB code 6Y84) of *coronavirus*; in cyan shading). Hydrogen bonds are highlighted by dashed lines, while hydrophobic interactions are represented by an arc.

Salvia is known as Murimia in Arabian and Kurdish and MaryCale in Persian literature. A Kurdish culinary recipe includes salvia as a functional tea, a tablespoon of salvia in a cup of hot water. Additionally, salvia has been used as an inhalator to treat respiratory system problems in Kurdish ethnomedicine. Based on our *in-silico* findings, phytocompounds reported in salvia showed more reliable BAs with 3CLpro in comparison to those of other plants reported in this order: oleanolic acid < *gamma*-elemene < ursolic acid < carnosol < ferruginol (Table 4).

Oleanolic acid, a pentacyclic triterpene, is found in the non-glyceride portion of olive pomace oil [46]. Pentacyclic triterpenes are natural ubiquitous phytocompounds that possess anti-inflammatory and antioxidative properties [46]. Oleanolic acid, glycyrrhizic acid, ursolic acid, and nomilin exhibited immunomodulatory effects [60]. Oleanolic acid, also known as caryophyllin, astrantiagenin C, giganteumgenin C, and virgaureagenin B, showed the best BA with 3CLpro in the present study and employed both hydrophobic interactions with all domains and hydrogen bonds with Gln299 and Asp295 residues of domain III of 3CLpro (Figure 4). In an influential review, antiviral effects of oleanolic acid and its derivatives against viral diseases such as influenza, hepatitis, human immune deficiency virus (HIV), and herpes viruses showed promising information based on *in vivo* and *in vitro* studies [61]. The drug-likeness of oleanolic acid is unacceptable because it violates Lipinski's rule of five due to high lipophilicity (≠ hydrophilicity), low hydrogen acceptivity, along with unsuitable pharmacokinetics parameters including low volume of distribution, zero unbound fraction of plasma protein, CYP3A4 substrate, and low total clearance (see supplementary file).

There was no report regarding the antiviral activity of **gamma-elemene**, a sesquiterpene [46]; however, it interacted hydrophobically with an array of amino acid residues of domain III of 3CLpro (Figure 4). Among all the compounds reported, gamma-elemene has the second and a reliable position in the BA with 3CLpro and which encourged us to dig deeper into its antiviral activity in future experimental studies. Indirect insecticidal [62] and larvicidal [63] activities of gamma-elemene were reported. Based on ADMET results, gamma-elemene follows the Lipinski's rule of five and hsd suitable pharmacokinetic parameters to be considered as a drug-like compound (see supplementary file).

Ursolic acid, a pentacyclic triterpenoid, is urs-12-*en*-28-oic acid substituted by a beta-hydroxyl moiety at position 3 and derives from a hydride of an ursane [46]. Various aspects of the antiviral potential of ursolic acid has been displayed in the rotavirus infection [64] and human papillomavirus-associated cervical cancer cells [65]. The various pharmacological properties of this dexamethasone-like structure has also been acknowledged in a ground-breaking patent review [66]. There was no report regarding the ant-SARS activity of ursolic acid, however it interacted hydrophobically with an array of amino acid residues of domain II and III of 3CLpro (Figure 4). Low hydrogen acceptivity, high lipophilicity, and the high topological polar surface area of ursolic acid violate the Lipinski's rule of five; however, it has very good intestinal absorption and zero unbound fraction of plasma protein. It has acceptable clearance in comparison to similar to its congener, oleanolic acid (see supplementary file).

Table 4. Computational binding affinities of major phytochemicals of *Salvia officinalis* with protease (PDB code 6Y84) of coronavirus

Ligand of PubChem; ID)	Binding affinity (Kcal/mol)	RMSD/UB	RMSD/LB
Carnosol 442009	-7.2	25.971	22.036
Ferruginol 442027	-7.1	47.766	45.165
Oleanolic acid 10494	-12.7	31.401	28.403
Ursolic acid 64945	-8.9	31.707	26.404
Gamma-elemene 6432312	-9.1	0.309	0.309

Note: RMSD: root mean-square deviation is the average distance between the atoms. UB: upper bound; LB: lower bound.

Carnosol is a diterpenoid compound which hydrophobically interacted with domain II and III of 3CLpro and also employed hydrogen bonds with Val303 residues of 3CLpro (Figure 4). Recently, reliable and BA -8.2 Kcal/mol of carnosol with active site of SARS-CoV-2 main protease has been reported in a high throughput *in silico* study [67]. Carnosol is naturally occurring in rosemary (*Rosemarinus officinalis*, Labiatae) and other the labiate herbs like sage. Its antioxidative activity has been reported [46]. Based on ADMET results, carnosol follows Lipinski's rule of five, but some of its pharmaco-kinetic parameters are not acceptable (see supplementary file).

Ferruginol is an abietane diterpenoid that is abieta-8,11,13-triene substituted by a hydroxy group at positions 12 [46]. Roa-Linares and coworkers [68] reported the antiviral effects of ferruginol analogues against human herpesvirus type 2, human herpesvirus type 1, and Dengue virus type 2. Ferruginol hydrophobically interacted by 3CLpro through a set of amino acid residues of domain II and III and also employed hydrogen bonds with Val303 residues of 3CLpro (Figure 4). Based on ADMET results, ferruginol also follows Lipinski's rule of five, but it would be considered as a HERG II inhibitor and potentially a cardiotoxic compound (see supplementary file).

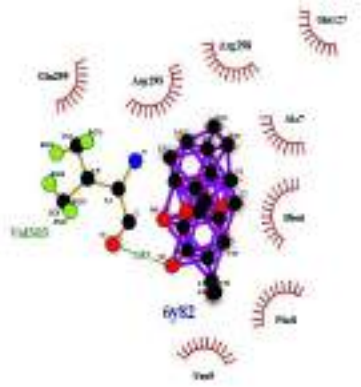

6y84

6Y84-Carnosol

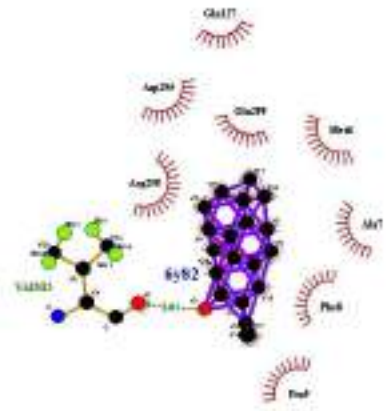

6y84

6Y84-Ferruginol

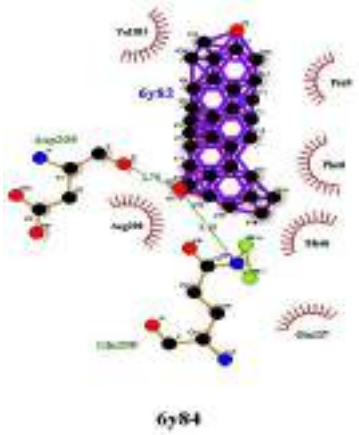

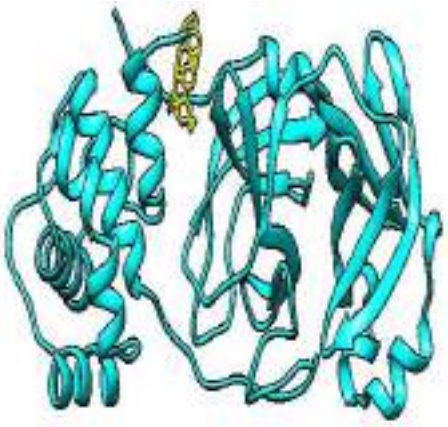

6Y84-Oleanolic acid

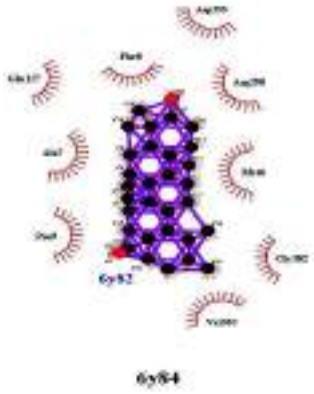

6Y84-Ursolic acid

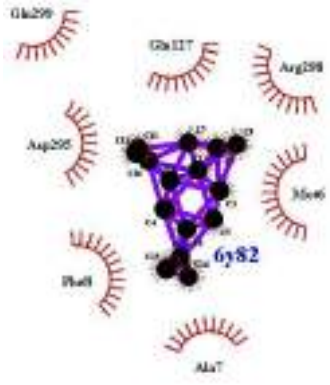

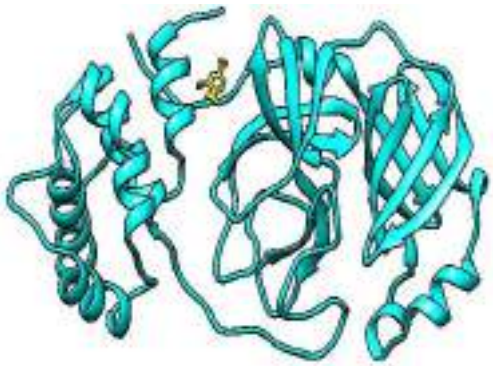

6Y84-*Gamma*-elemene

Figure 4. Molecular docking of phytocompounds of *Salvia officinalis* (in yellow shading against protease (PDB code 6Y84) of *coronavirus*; in cyan shading). Hydrogen bonds are highlighted by dashed lines, while hydrophobic interactions are represented by an arc.

Ginger, also called Alzanjabil in Mesopotamia, Zanjafel in Kurdish, and Zyngbir in Persian traditional medicine, is usually used in the form of pieces or powder. Ginger is used as a tea, food additive, or a safe food by U.S. Food and Drug Administration which has invigorated people to use it more frequently. Among the phytochemicals of ginger, (E)-γ-Bisabolene has the strongest BA with 3CLpro through a set of amino acid residues of domain II and III (Figure 5; Table 5). This sesquiterpene compound is found in anise [46] and ginger and is known as a flavoring agent in the market. As far as we could possibly know, no trustful antiviral action of this bisabolene has been accounted for, but its antitumor effect has been researched [69]. Based on ADMET results, (E)-γ-Bisabolene is lipophilic and can cross the lipid membrane easily, however its low water solubility may interfere with its volume distribution (see supplementary file).

Beta-curcumene, a sesquiterpene [46], hydrophobically interacted with domain II and III of 3CLpro (Figure 5) and its pharmacological properties remain unknown. In addition to its presence in ginger, **(S)-Phellandral** is a constituent of *Anethum sowa* (Indian dill) [46]. The (S)-Phellandral hydrophobically interacted with 3CLpro and also bound to 3CLpro through hydrogen bonds with the Gln127 residue of domain II and III of 3CLpro (Figure 5). No overt violation against Lipinski's rule of five was detected for *β*-curcumene and (S)-Phellandral and they have suitable pharmacokinetic parameters except low water solubility to be considered as lead-like compounds (see supplementary file). Similar to beta-curcumene, pharmacological properties of (S)-Phellandral remain unknown.

Table 5. Computational binding affinities of major phytochemicals of *Zingiber officinale* with protease (PDB code 6Y84) of coronavirus

Ligand of PubChem; ID)	Binding affinity (Kcal/mol)	RMSD/UB	RMSD/LB
Phellandral 89488	-7.1	1.921	1.413
β-Curcumene 6428461	-7.5	1.518	0.867
(E)-γ-Bisabolene 5352437	-8.0	2.619	2.067

Note: RMSD: root mean-square deviation is the average distance between the atoms. UB: upper bound; LB: lower bound.

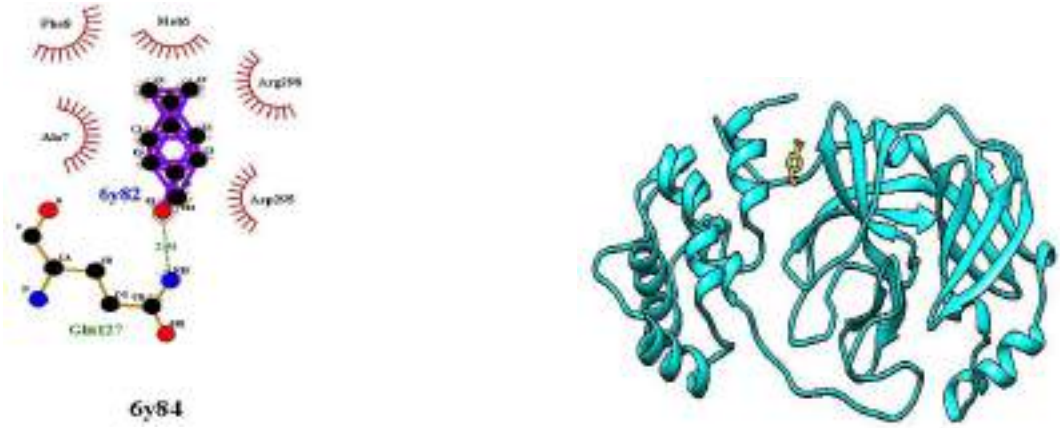

6Y84-Phellandral

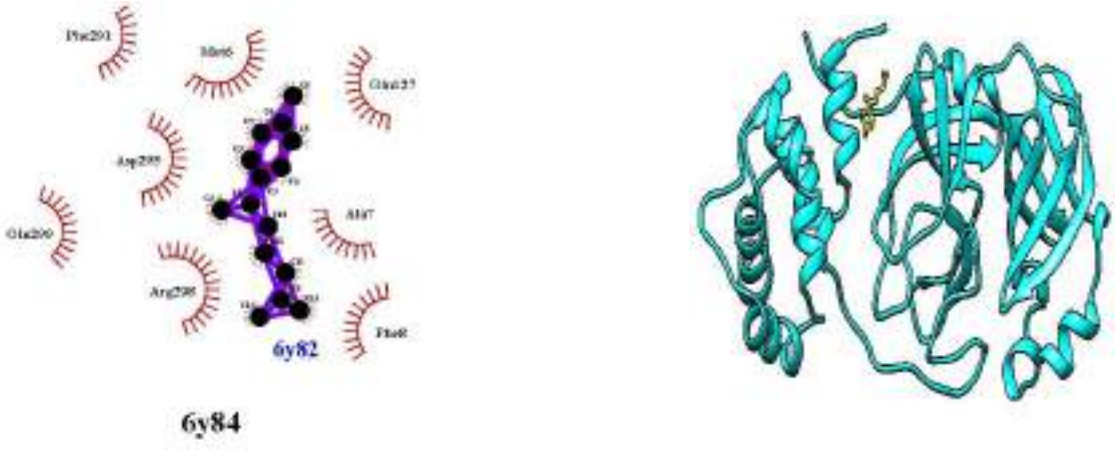

6Y84-*β*-Curcumene

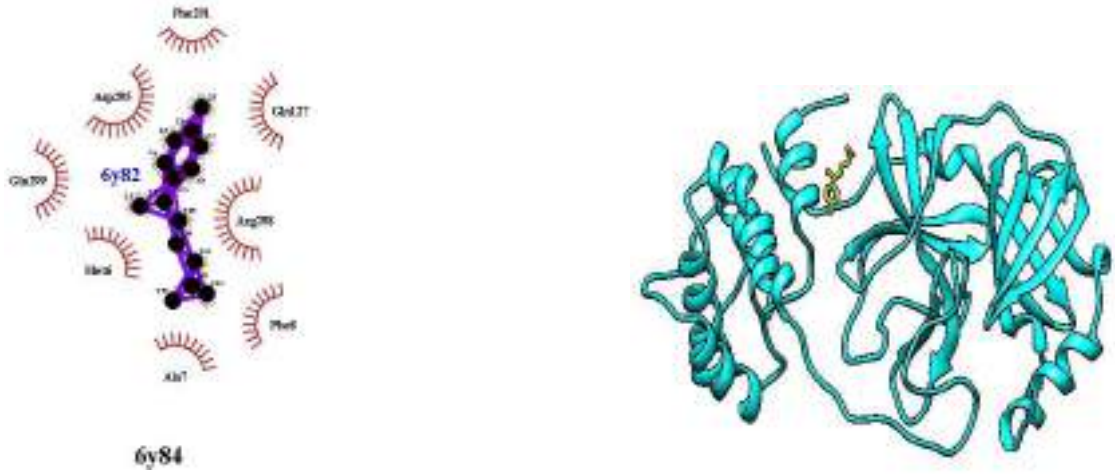

6Y84-(E)-γ-Bisabolene

Figure 5. Molecular docking of phytocompounds of *Zingiber officinale* (in yellow shading) with protease (PDB code 6Y84) of *coronavirus*; in cyan shading). Hydrogen bonds are highlighted by dashed lines, while hydrophobic interactions are represented by an arc.

SUMMARY

- Coronavirus disease 2019 (COVID-19) is a contagion caused by severe acute respiratory *syndrome coronavirus* 2 (SARS-CoV-2) which led to huge socioeconomic losses throughout the world. The pathogenesis of COVID-19 has yet to be cleared, while its high mutation rate led to the high mor-bidity and mortality of this (re)emergent disease which further limits the effectiveness of routine preventive and therapeutic recipes.
- Kurdish ethnomedicine developed around the Zagros mountains and Mesopotamia where their in-habitants experienced many ancient and modern pandemics throughout millennia. Therefore, we screened the botanical formulations used for preparing antipyretic (putative orthodox antiviral) rec-ipes throughout history. Hence, the objective of this chapter was to find evidence of possible anti-SARS-CoV-2 activity in Kurdish recipes by deciphering the binding affinity (BA; kcal/mol; *vide infra* in the parentheses) of screened phytochemicals to targ3CLpro (PDB:6Y84) *in silico*.

- We screened fenugreek (*Trigonella foenum-graecum*), chamomile (*Matricaria chamomilla*), sage (*Salvia officinalis*), and ginger (*Zingiber officinale*) through a rapid survey of traditional herbalists and reviews of remnant literature of the Kurdish people. In brief, an antipyretic recipe was a boiled drink prepared from fenugreek seeds which was prescribed twice per day and a small spoon of fenugreek powder mixed with a tablespoon of honey. Other recipes contained one tablespoon of squeezed orange exhausted to some hot chamomile tea and a little spoon of ginger powder blended in with some hot chamomile tea.
- A culinary recipe of salvia was its tea or a tablespoon of salvia blended with heated water. Other recipes contained chips or powder of ginger used as a tea or a food additive. More notably, salvia has been used in the form of steam inhalation to treat respiratory disorders like acute respiratory distress syndrome (ARDS) caused by COVID-19.
- The results of molecular docking showed that diosgenin (-8.9), rhaponticin (-8.3), and isovitexin (-7.6) found in fenugreek; luteolin-7-*O*-glucoside (-9.1), apigenin-7-*O*-glucoside (-8.9), quercetin (-8.1), luteolin (-7.9), chlorogenic acid (-9.2), matricin (-7.1), and caffeic acid (-7.0) found in chamomile; oleanolic acid (-12.7), *gamma*-elemene (-9.1), ursolic acid (-8.9), carnosol (-7.2), and ferruginol (-7.1) found in sage; and (E)-γ-bisabolene (-8.0), *β*-curcumene (-7.5), and phellandral (-7.1) found in ginger have reliable BA < -7.0 kcal/mol and can be considered as putative strong protease binders including loop and domain binders.
- Moreover, experimental investigations supported the previously strict antiviral activities of *β*-cur-cumene, ferruginol, carnosol, ursolic acid, oleanolic acid, caffeic acid, chlorogenic acid, luteolin, quercetin, luteolin-7-*O*-glucoside, diosgenin, and isovitexin.
- In sum, oleanolic acid, chlorogenic acid, and luteolin-7-*O*-glucoside can be considered as *hit* molecules of this computational effort which should be submitted to quantitative structure activity relationship (QSAR) analyses and *similarity research* against protease *in silico* and *in vitro*.
- Cautiously, sage is an ethnic gift of Kurdish ethnomedicine for the prevention and treatment of COVID-19 if prescribed by Kurdish herbalists and we encourage clinicians to prescribe it as a *functional tea* or an inhaler for patients and medical recruits.

TEST QUESTIONS

1. Which plant has been used as an inhalator to treat respiratory disorders like acute respiratory distress syndrome (ARDS) in Kurdish ethnomedicine:
    a. Fenugreek
    b. Sage
    c. Chamomile
    d. Ginger
2. Which plant contains the most promising functional ingredients against COVID-19 in this study
    a. Fenugreek
    b. Chamomile
    c. Sage
    d. Ginger
3. Lipinski's rule of five [70] varies based on
    a. hydrogen bond donors < 5; hydrogen bond acceptors < 10
    b. An octanol-water partition coefficient (log P) < 5
    c. A molecular mass < 500 daltons
    d. All of the above
4. Which phytocompounds inhibited as profen in this study?
    a. Physical performance

b. Mitricin
c. Organ or system function
d. Cognitive, behavioral, and psychological function

5. Based on *in silico* effort of the present study, which of the following phytocompounds showed the best docking with 3CLpro?
    a. Oleanolic Acid
    b. *Gamma*-elemene
    c. Luteolin-7-*O*-glucoside
    d. Rhaponticin

Answers: 1:(B) 2:(C) 3:(D) 4:(B) 5:(A)

REFERENCES:

1. Mimica-Dukić, N (2013) The Healing Power of Herbs and Phytotherapy Today Chpt. in: "Plants and Herbs in Traditional Serbian Culture, Handbook of folk botany," Editors Zoja Karanović & Jasmina Jokić. p.119. Ivana Živančević Sekeruš. ISBN 978-86-6065-172-5
2. Pieroni, A., Ahmed, H. M., & Zahir, H. (2017). The spring has arrived: traditional wild vegetables gathered by Yarsanis, Ahl-e Haqq and Sunni Muslims in Western Hawraman, SE Kurdistan, Iraq. Acta Societatis Botanicorum Poloniae, 86(1).
3. Yang H, Xie W, Xue X, Yang K, Ma J, Liang W, et al. (2005). Design of wide-spectrum inhibitors targeting coronavirus main proteases. PLoS Biol, (3)324.
4. Pillaiyar, T., Manickam, M., Namasivayam, V., Hayashi, Y., & Jung, S. H. (2016). An overview of severe acute respiratory syndrome–coronavirus, SARS-CoV 3CL protease inhibitors: peptidomimetics and small molecule chemotherapy. Journal of medicinal chemistry, 59(14), 6595-6628.
5. Wu C, Liu Y, Yang Y, Zhang P, Zhong W, Wang Y, Wang Q, Xu Y, Li M, Li X, Zheng M, Chen L, Li H. (2020). Analysis of therapeutic targets for SARS-CoV-2 and discovery of potential drugs by computational methods. Acta Pharmaceutica Sinica B, 10(5), 766-788.
6. Khan, SA., Zia, K., Ashraf, S., Uddin, R., & Ul-Haq, Z. (2020) Identification of chymotrypsin-like protease inhibitors of SARS-CoV-2 via integrated computational approach. Journal of Biomolecular Structure and Dynamics, (1)13.
7. Bahmani, M., Shirzad, H., Mirhosseini, M., Mesripour, A., & Rafieian-Kopaei, M. (2016). A review on ethnobotanical and therapeutic uses of fenugreek (*Trigonella foenum-graceum* L). Journal of Evidence-Based Complementary & Alternative Medicine, 21(1), 53-62.
8. Anter, J., Romero-Jiménez, M., Fernández-Bedmar, Z., Villatoro-Pulido, M., Analla, M., Alonso-Moraga, A., & Muñoz-Serrano, A. (2011). Antigenotoxicity, cytotoxicity, and apoptosis induction by apigenin, bisabolol, and protocatechuic acid. Journal of Medicinal Food, 14(3), 276-283.
9. Rahmani, M., Hamel, L., Toumi-Benali, F., Dif, M. M., Moumen, F., & Rahmani, H. (2018). Determination of antioxidant activity, phenolic quantification of four varieties of fenugreek *Trigonella foenum graecum* L. seed extract cultured in west Algeria. J Mater Environ Sci, 9(6), 1656-1661.
10. Sulieman, A. M. E., Ahmed, H. E., & Abdelrahim, A. M. (2008). The chemical composition of fenugreek (*Trigonella foenum-graceum* L) and the antimicrobial properties of its seed oil. Gezira J. of Eng & Applied Sci, 3(2), 52-71.
11. Balbontín, Y. M., Stewart, D., Shetty, A., Fitton, C. A., & McLay, J. S. (2019). Herbal medicinal product use during pregnancy and the postnatal period: a systematic review. Obstetrics and gynecology, 133(5), 920.
12. Kaviarasan, S., Vijayalakshmi, K., & Anuradha, C. V. (2004). Polyphenol-rich extract of fenugreek seeds protect erythrocytes from oxidative damage. Plant Foods for Human Nutrition, 59(4), 143-147.
13. Mehrafarin, A., Rezazadeh, S. H., Naghdi Badi, H., Noormohammadi, G. H., Zand, E., & Qaderi, A. (2011). A review on biology, cultivation and biotechnology of fenugreek (*Trigonella foenum-graecum* L.) as a valuable medicinal plant and multipurpose. J. Med. Plants, 10(37), 6-24.
14. Aboubakr, H. A., Nauertz, A., Luong, N. T., Agrawal, S., El-Sohaimy, S. A., Youssef, M. M., & Goyal, S. M. (2016). In vitro antiviral activity of clove and ginger aqueous extracts against feline calicivirus, a surrogate for human norovirus. Journal of food protection, 79(6), 1001-1012.
15. Smith, M. (2003). Therapeutic applications of fenugreek. Alternative Medicine Review, 8(1), 20-27.
16. Shukla, K. M., Shukla, A. K., & Shukla, M. M. (2011). U.S. Patent Application No. 12/800, 553.
17. Wani, S. A., & Kumar, P. (2018). Fenugreek: A review on its nutraceutical properties and utilization in various food products. Journal of the Saudi Society of Agricultural Sciences, 17(2), 97-106.

18. Rasheed, M. S. A. A., Wankhade, M. V., Saifuddin, M. S. S. K., & Sudarshan, M. A. R. (2015). Physico-chemical properties of fenugreek (*Trigonella foenum-graceum* L) seeds. International Journal of Engineering Research & Technology, 4(9).
19. Singh, O., Khanam, Z., Misra, N., & Srivastava, M. K. (2011). Chamomile (*Matricaria chamomilla* L): an overview. Pharmacognosy Reviews, 5(9), 82.
20. Mawlood, S. I. (2011). Chemical and biological study of Iraqi Kurdistan chamomile flower (*Matricaria recutita* L). Baghdad Science Journal, 8(3), 736-740.
21. Chalechale, A., Karimi, I., Zavareh, S., & Karimi, A. (2013). Brief anthropology and antiparasitic remedies in Kurdish ethno (Veterinary) Medicine: A neglected treasure trove. World's Veterinary Journal, 3, 29-32.
22. Chiru, T., Fursenco, C., Ciobanu, N., Dinu, M., Popescu, E., Ancuceanu, R., Daisy, V., & Raal, A. (2020). Use of medicinal plants in complementary treatment of the common cold and influenza–perception of pharmacy customers in Moldova and Romania. Journal of Herbal Medicine, 100346.
23. Ghanipour, A., Ali, A. M., & Karimi, I. (2011). Protective effect of pomegranate on paracetamol-induced hepatotoxicity in rats. Clinical Biochemistry, 44(13), S350-S351.
24. Hamidpour, M., Hamidpour, R., Hamidpour, S., & Shahlari, M. (2014). Chemistry, pharmacology, and medicinal property of sage (Salvia) to prevent and cure illnesses such as obesity, diabetes, depression, dementia, lupus, autism, heart disease, and cancer. Journal of traditional and complementary medicine, 4(2), 82-88.
25. Geuenich, S., Goffinet, C., Venzke, S., Nolkemper, S., Baumann, I., Plinkert, P., ... & Keppler, O. T. (2008). Aqueous extracts from peppermint, sage and lemon balm leaves display potent anti-HIV-1 activity by increasing the virion density. Retrovirology, 5(1), 27.
26. Sertel, S., Eichhorn, T., Plinkert, P. K., & Efferth, T. (2011). Anticancer activity of Salvia officinalis essential oil against HNSCC cell line (UMSCC1). Hno, 59(12), 1203-1208.
27. Bonesi, M., Loizzo, M. R., Acquaviva, R., Malfa, G. A., Aiello, F., & Tundis, R. (2017). Anti-inflammatory and antioxidant agents from Salvia genus (Lamiaceae): An assessment of the current state of knowledge. Anti-Inflammatory & Anti-Allergy Agents in Medicinal Chemistry, 16(2), 70-86.
28. Ahmed, H. M. (2016). Ethnopharmacobotanical study on the medicinal plants used by herbalists in Sulaymaniyah Province, Kurdistan, Iraq. Journal of Ethnobiology and Ethnomedicine, 12(1), 8.
29. Šmidling, D., MITIć-ćULAfIć, D. R. A. G. A. N. A., VUkOVIć-GAčIć, B., Simić, D., & Knežević-Vukčević, J. (2008). Evaluation of antiviral activity of fractionated extracts of sage *Salvia officinalis* L.(Lamiaceae). Archives of Biological Sciences, 60(3), 421-429.
30. Khan, M. T. H., Ather, A., Thompson, K. D., & Gambari, R. (2005). Extracts and molecules from medicinal plants against herpes simplex viruses. Antiviral Research, 67(2), 107-119.
31. Zgorniak-Nowosielska, I., Zawilinska, B., Manolova, N., & Serkedjieva, J. (1989). A study on the antiviral action of a polyphenolic complex isolated from the medicinal plant Geranium sanguineum L. VIII. Inhibitory effect on the reproduction of herpes simplex virus type 1. Acta Microbiologica Bulgarica, 24, 3-8.
32. Ghorbani, A., & Esmaeilizadeh, M. (2017). Pharmacological properties of *Salvia officinalis* and its components. Journal of Traditional and Complementary Medicine, 7(4), 433-440.
33. Khalil, R., & Li, Z. G. (2011). Antimicrobial activity of essential oil of *Salvia officinalis* L. collected in Syria. African Journal of Biotechnology, 10(42), 8397-8402.
34. Ahmed, K., Shaheen, G., & Asif, H. M. (2011). *Zingiber officinale* Roscoe (pharmacological activity). Journal of Medicinal Plants Research, 5(3), 344-348.
35. Platel, K., & Srinivasan, K. (1996). Influence of dietary spices or their active principles on digestive enzymes of small intestinal mucosa in rats. International journal of food sciences and nutrition, 47(1), 55-59.
36. Denyer, C. V., Jackson, P., Loakes, D. M., Ellis, M. R., & Young, D. A. (1994). Isolation of antirhinoviral sesquiterpenes from ginger (*Zingiber officinale*). Journal of Natural Products, 57(5), 658-662.
37. Ernst, E., & Pittler, M. H. (2000). Efficacy of ginger for nausea and vomiting: a systematic review of randomized clinical trials. British Journal of Anaesthesia, 84(3), 367-371.
38. Abdul, A. B. H., Al-Zubairi, A. S., Tailan, N. D., Wahab, S. I. A., Zain, Z. N. M., Ruslay, S., & Syam, M. M. (2008). Anticancer activity of natural compound (Zerumbone) extracted from *Zingiber zerumbet* in human HeLa cervical cancer cells. International Journal of Pharmacology, 4(3), 160-168.
39. Tian, L. Q., Huang, H. G., Ye, X. C., Li, N., Zou, T., Zhou, A. J., & Liu, Y. W. (2012). Anti-influenza virus activity and chemical composition of *Ramulus Cinnamomi-Ramulus Zingiber Recens*, a Chinese herb pair. Chinese Journal of Hospital Pharmacy, 2012(14), 9.
40. Liu, Y., Liu, J., & Zhang, Y. (2019). Research progress on chemical constituents of *Zingiber officinale* Roscoe. BioMed Research International, 2019,1-21.
41. Dallakyan, S., & Olson AJ. (2015). Small-molecule library screening by docking with PyRx. Methods Mol Biol J, 1263, 243–250.

42. Thomsen, R., & Christensen, MH. (2006). Mol Dock: a new technique for high–accuracy molecular docking. J Med Chem, 49(11), 3315–3321.
43. Laskowski, RA., & Swindells, MB. (2011). Ligplot+: multiple ligand–protein interaction diagrams for drug discovery. J Chem Inf Model, 51(10), 2778–2786.
44. Du, Q., Mezey, PG., & Chou, KC. (2005). Heuristic molecular lipophilicity potential (HMLP): a 2D-QSAR study to LADH of molecular family pyrazole and derivatives. J Comput Chem, 26(5), 461–470.
45. Cheng, F., Li, W., Zhou, Y., Shen, J., Wu, Z., Liu, G., Lee, PW., & Tang, Y. (2012). AdmetSAR: a comprehensive source and free tool for assessment of chemical ADMET properties. J Chem Inf Model, 52(11), 3099-105.
46. PubChem Database. (2020). National Center for Biotechnology Information. https://pubchem.ncbi.nlm.nih.gov/compound.
47. Jesus, M., Martins, APJ., Gallardo, E., & Silvestre, S. (2016). Diosgenin: recent highlights on pharmacology and analytical methodology. Journal of Analytical Methods in Chemistry, 2016, 1-16.
48. Wang, YJ., Pan, KL., Hsieh, TC., Chang, TY., Lin, WH., & Hsu, JTA. (2011). Diosgenin, a plant-derived sapogenin, exhibits antiviral activity in vitro against hepatitis C virus. Journal of Natural Products, 4(74), 580–584.
49. Kolodziejczyk-Czepas, J., Czepas, J. (2019). Rhaponticin as an anti-inflammatory component of rhubarb: a minireview of the current state of the art and prospects for future research. Phytochem Rev 18, 1375–1386.
50. Xiao, J., Capanoglu, E., Jassbi, AR., & Miron, A. (2016). Advance on the flavonoid c-glycosides and health benefits. Critical Reviews in Food Science and Nutrition, 56, S29-S45.
51. Cui, XX., Yang, X., Wang, HJ., Rong, XY., Jing, S., Xie, YH., Huang, DF., & Zhao, C. (2017). Luteolin-7-O-glucoside present in lettuce extracts inhibits hepatitis b surface antigen production and viral replication by human hepatoma cells in vitro. Front Microbiol, 2425.
52. Fan, W., Qian, S., Qian, P., & Li, X. (2016). Antiviral activity of luteolin against Japanese encephalitis virus. Virus Res, 220,112-116.
53. Zakaryan, H., Arabyan, E., Oo, A., Zandi, K. (2107). Flavonoids: promising natural compounds against viral infections. Archives of Virology,162(9), 2539-2551.
54. Ding, Y., Cao, Z., Cao, L., Ding, G., Wang, Z., & Xiao, W. (2107). Antiviral activity of chlorogenic acid against influenza A (H1N1/H3N2) virus and its inhibition of Neuraminidase. Scientific Reports,7,45723.
55. Ramadan, M., Goeters, S., Watzer, B., Krause, E., Lohmann, K., Bauer, R., Hempel, B., Imming, P. (2006). Chamazulene carboxylic acid and matricin: a natural profen and its natural prodrug, identified through similarity to synthetic drug substances. J Nat Prod, 69(7), 1041-1045.
56. Utsunomiya, H., Ichinose, M., Ikeda, K., Uozaki, M., Morishita, J., Kuwahara, T., Koyama, AH., Yamasaki, H. (2014). Inhibition by caffeic acid of the influenza A virus multiplication in vitro. International Journal of Molecular Medicine, 34, 1020-1024.
57. Ogawa, M., Shirasago,Y., Ando,S., Shimojima, M., Saijo, M., Fukasawa, M. (2018). Caffeic acid, a coffee-related organic acid, inhibits infection by severe fever with thrombocytopenia syndrome virus in vitro. Journal of Infection and Chemotherapy, 4, 597-601.
58. Yao Li, Y., Yao, J., Han, C., Yang, J., Chaudhry, MT., Wang, S., Liu, H., &Yin, Y. (2016). Quercetin, inflammation and immunity. Nutrients, 8(3), 167.
59. Wu, W., Li, R., Li, X., He, J., Jiang, S., Liu, S., & Yang, J. (2015). Quercetin as an antiviral agent inhibits influenza A virus (IAV) Entry. Viruses, 8(1), 6.
60. Raphael, TJ., & Kuttan, G. (2003). Effect of naturally occurring triterpenoids glycyrrhizic acid, ursolic acid, oleanolic acid and nomilin on the immune system. Phytomedicine, 10(6-7), 483-489.
61. Khwaza, V., Oyedeji, OO., & Aderibigbe, BA. (2018). Antiviral activities of oleanolic acid and its analogues. Molecules, 23(9), 2300.
62. Benelli, G., Govindarajan, M., AlSalhi, MS., Devanesan, S., & Maggi, F. (2018). High toxicity of camphene and γ-elemene from *Wedelia prostrata* essential oil against larvae of *Spodoptera litura* (Lepidoptera: Noctuidae). Environ Sci Pollut Res Int., 25(11), 10383-10391.
63. Govindarajan , M., Rajeswary, M., Senthilmurugan , S., Vijayan, P., Alharbi, NS., Shine Kadaikunnan, S., Khaled , JM., & Benelli , G. (2018). Curzerene, trans-β-elemenone, and γ-elemene as effective larvicides against *Anopheles subpictus*, *Aedes albopictus*, and *Culex tritaeniorhynchus*: toxicity on non-target aquatic predators. Environ Sci Pollut Res Int., 25(11), 10272-10282.
64. Tohme, MJ., Gimenez, MC., Peralta, A., Colombo, MI., & Delgui, LR. (2019). Ursolic acid: A novel antiviral compound inhibiting rotavirus infection in vitro. Int J Antimicrob Agents, 54(5), 601-609.
65. Yim , EK., Lee, MJ., Lee, KH., Um, SJ., & Park, JS. (2006). Antiproliferative and antiviral mechanisms of ursolic acid and dexamethasone in cervical carcinoma cell lines. Int J Gynecol Cancer, 16(6), 2023-31.
66. Hussain, H., Green, IR., Ali, I., Khan, IA., Ali, Z., Al-Sadi, AM., & Ahmed, I. (2017). Ursolic acid derivatives for pharmaceutical use: a patent review (2012-2016). Expert Opin Ther Pat, 27(9), 1061-1072.

67. Umesh, Kundu, D., Selvaraj, C., Singh, SK., & Dubey, VK. (2020). Identification of new anti-nCoV drug chemical com-pounds from Indian spices exploiting SARS-CoV-2 main protease as target. J Biomol Struct Dyn., 1-9.
68. Roa-Linares, VC., Brand, YM., Agudelo-Gomez, LS., Tangarife-Castaño, V., Betancur-Galvis, LA., Gomez, GJC., Gon-zález, MA. (2015). Anti-herpetic and anti-Dengue activity of abietane ferruginol analogues synthesized from (+)-dehy-droabietylamine. Eur J Med Chem,108,79-88.
69. Jou, YJ., Hua, CH., Lin, CS., Wang, CY., Wan, L., Lin, YJ., Huang, HS., & Lin, CW. (2016). Anticancer activity of γ-bisabolene in human neuroblastoma cells via induction of p53-mediated mitochondrial apoptosis. Molecules, 21(5), 601.
70. Lipinski, CA., Lombardo, F., Dominy, BW., & Feeney, PJ. (2001). Experimental and computational approaches to esti-mate solubility and permeability in drug discovery and development settings. Advanced Drug Delivery Reviews, 46 (1–3), 3–26.